J|A|C|S ARTICLES

Published on Web 07/07/2009

Synthesis, Characterization, and Photoinduced Electron Transfer Processes of Orthogonal Ruthenium Phthalocyanine−Fullerene Assemblies

M. Salomé Rodríguez-Morgade,[†] Marta E. Plonska-Brzezinska,[‡] Andreas J. Athans,[‡] Esther Carbonell,[§] Gustavo de Miguel,[§] Dirk M. Guldi,*[,§] Luis Echegoyen,*[,‡] and Tomás Torres*[,†]

Departamento de Química Orgánica (C-I), Universidad Autónoma de Madrid, Cantoblanco, E-28049 Madrid, Spain, Institute for Physical Chemistry, Friedrich-Alexander-Universität Erlangen-Nürnberg, Egerlandstrasse 3, D-91058 Erlangen, Germany, and Department of Chemistry, Clemson University, Clemson, South Carolina 29634

Received March 27, 2009; E-mail: tomas.torres@uam.es; dirk.guldi@chemie.uni-erlangen.de; luis@CLEMSON.EDU

Abstract: The convergent synthesis, electrochemical characterization, and photophysical studies of phthalocyanine−fullerene hybrids **3**−**5** bearing an orthogonal geometry (Chart 2) are reported. These donor−acceptor arrays have been assembled through metal coordination of linear fullerene mono- and bispyridyl ligands to ruthenium(II) phthalocyanines. The hybrid [Ru(CO)(C_{60}Py)Pc] (**3**) and the triad [Ru_2(CO)$_2$($C_{60}Py_2$)Pc_2] (**5**) were prepared by treatment of the phthalocyanine **6** with the mono- and hexakis-substituted C_{60}−pyridyl ligands **1** and **2**, respectively. The triad [Ru($C_{60}Py)_2$Pc] (**4**) was prepared in a similar manner from the monosubstituted C_{60}−pyridyl ligand **1** and the phthalocyanine precursor **7**. The simplicity of this versatile synthetic approach allows to determine the influence of the donor and acceptor ratio in the radical ion pair state lifetime. The chemical, electrochemical, and photophysical characterization of the phthalocyanine−fullerene hybrids **3**−**5** was conducted using ^{1}H and ^{13}C NMR, UV/vis, and IR spectroscopies, as well as mass spectrometry, cyclic voltammetry, femtosecond transient absorption studies, and nanosecond laser flash photolysis experiments. Arrays **3**−**5** exhibit electronic coupling between the two electroactive components in the ground state, which is modulated by the axial CO and 4-pyridylfulleropyrrolidine ligands. With respect to the excited state, we have demonstrated that RuPc/C_{60} electron donor−acceptor hybrids are a versatile platform to fine-tune the outcome and dynamics of charge transfer processes. The use of ruthenium(II) phthalocyanines instead of the corresponding zinc(II) complexes allows the suppression of energy wasting and unwanted charge recombination, affording radical ion pair state lifetimes on the order of hundreds of nanoseconds for the C_{60}-monoadduct-based complexes **3** and **4**. For the hexakis-substituted C_{60} unit **2**, the reduction potential is shifted cathodically, thus raising the radical ion pair state energy. However, the location of the RuPc triplet excited state is not high enough, and still offers a rapid deactivation of the radical ion pair state.

Introduction

In the field of sustainable energy production, solar power technologies are emerging as one of the most promising alternatives. The concept relies on the fact that sunlight constitutes the initial energetic source for a colossal chain of interdependent biological events, making possible life as we know it. Therefore, developing efficient and affordable systems, able to harvest, convert, and store sunlight, is considered a very desirable approach toward obtaining clean energy, and these inventions are limited only by human ingeniousness.[1,2] The design of such complex devices is often rationalized by applying the "modular approach",[3] which consists in constructing multicomponent artificial arrays of three or more units, able to perform each of the natural photosynthetic key steps (i.e., capture of visible light photons and electron transfer to afford energetic oxidizing and reducing equivalents with long lifetimes of ∼1 s).[4] These constructs are useful in artificial-photosynthesis research as well as photovoltaic and optoelectronic applications.

Owing to their preeminent role in nature, porphyrinoids are the usual chromophores of choice to be employed as components

[†] Universidad Autónoma de Madrid.
[‡] Clemson University.
[§] Friedrich-Alexander-Universität Erlangen-Nürnberg.

(1) *Artificial Photosynthesis: From Basic Biology to Industrial Application*; Collings, A. F., Critchley, C., Eds.; Wiley-VCH Verlag GmbH & Co. KGaA: Weinheim, Germany, 2005; 313 pp.

(2) (a) Wasielewski, M. R. *Chem. Rev.* **1992**, *92*, 435–461. (b) Gust, D.; Moore, T. A.; Moore, A. L. *Acc. Chem. Res.* **2001**, *34*, 40–48. (c) Arakawa, H.; et al. *Chem. Rev.* **2001**, *101*, 953–996. (d) Chakraborty, S.; Wadas, T. J.; Hester, H.; Schmehl, R.; Eisenberg, R. *Inorg. Chem.* **2005**, *44*, 6865–6878. (e) Balzani, V.; Clemente-León, M.; Credi, A.; Ferrer, B.; Venturi, M.; Flood, A. H.; Stoddart, J. F. *Proc. Natl. Acad. Sci. U.S.A.* **2006**, *103*, 1178–1183.

(3) (a) Eisenberg, R.; Nocera, D. G. *Inorg. Chem.* **2005**, *44*, 6799–6801, and references therein. (b) *Artificial Mimicry of Photosynthesis*; Thayyumanavan, S., Ed. *Photosynth. Res.* **2006**, *87* (1), 150 pp.

 10.1021/ja902471w CCC: $40.75

of such photovoltaic and artificial photosynthetic devices.[2a,5−7] The advantages of these macrocycles over other types of molecules arise from their 18 π electron aromatic structure that confers them high molar absorption coefficients and fast energy and/or electron transfer abilities to the acceptor components of the system. In addition, the possibility to endow these compounds with a range of redox potentials by simple introduction of different central metals and/or peripheral substituents[8] constitutes an appealing feature for their use in the design of artificial devices.

Phthalocyanines are among the synthetic porphyrin analogues that exhibit the most promising properties for application in solar technologies.[6a,9,10] They show excellent light-harvesting capabilities over a wide range of the solar light spectrum, with a maximum around 700 nm, where the maximum of the solar photon flux occurs.[11] In this respect, while regular porphyrins do not display significant absorption at energies lower than 550 nm,[11] the development of systems that absorb a substantial portion of the solar spectrum should bring about a major advance in the field. Phthalocyanines also produce efficient electron transfer processes that can be regulated by the appropriate choice of the central metal and the nature of the peripheral substitution.[12,13] Finally, rapid CS and slow CR rates are facilitated by the small reorganization energies of electron transfer that these chromophores exhibit.[14]

Our extensive experience in the design of phthalocyanine-based derivatives for optoelectronic applications has led us to use the Pc macrocycle as a component of diverse electron donor−acceptor conjugates and/or hybrids.[13e,14a,15] Among them, the phthalocyanine−fullerene motif has been the object of more profound studies. The incorporation of the fullerene structure as the oxidizing component of donor−acceptor systems has often resulted in the acceleration of the intramolecular CS process and a deceleration of the CR. These effects have been attributed to the rigid and confined structure of the C_{60} aromatic π sphere, which leads to smaller reorganization energy, as compared to other types of acceptors, such as the planar quinones and imides.[7b,16] Accordingly, we have designed a considerable number of covalently linked phthalocyanine−

(4) (a) *The Photosynthetic Reaction Center*; Deisenhofer, J., Norris, J. R., Eds.; Academic Press: New York, 1993. (b) *Molecular Mechanisms of Photosynthesis*; Blankenship, R. E., Ed.; Blackwell Science: Malden, MA, 2002. (c) McEvoy, J. P.; Brudvig, G. W. *Chem. Rev.* **2006**, *106*, 4455–4483.

(5) (a) Moore, G. F.; Hambourger, M.; Gervaldo, M.; Poluektov, O. G.; Rajh, T.; Gust, D.; Moore, T. A.; Moore, A. L. *J. Am. Chem. Soc.* **2008**, *130*, 10466–10467. (b) Rizzi, A. C.; van Gastel, M.; Liddell, P. A.; Palacios, R. E.; Moore, G. F.; Kodis, G.; Moore, A. L.; Moore, T. A.; Gust, D.; Braslavsky, S. E. *J. Phys. Chem. A* **2008**, *112*, 4215–4223. (c) Fukuzumi, S.; Kojima, T. *J. Mater. Chem.* **2008**, *18*, 1427–1439. (d) Kelley, R. F.; Lee, S. J.; Wilson, T. M.; Nakamura, Y. i.; Tiede, D. M.; Osuka, A.; Hupp, J. T.; Wasielewski, M. R. *J. Am. Chem. Soc.* **2008**, *130*, 4277–4284. (e) Benniston, A. C. *Phys. Chem. Chem. Phys.* **2007**, *9*, 5739–5747. (f) Nakamura, Y.; Aratani, N.; Osuka, A. *Chem. Soc. Rev.* **2007**, *36*, 831–845.

(6) (a) Satake, A.; Kobuke, Y. *Org. Biomol. Chem.* **2007**, *5*, 1679–1691. (b) Gadde, S.; Islam, D.-M. S.; Wijesinghe, C. A.; Subbaiyan, N. K.; Zandler, M. E.; Araki, Y.; Ito, O.; D'Souza, F. *J. Phys. Chem. C* **2007**, *111*, 12500–12503. (c) Sanchez, L.; Sierra, M.; Martin, N.; Myles, A. J.; Dale, T. J.; Rebek, J., Jr.; Seitz, W.; Guldi, D. M. *Angew. Chem., Int. Ed.* **2006**, *45*, 4637–4641. (d) Schuster, D. I.; Li, K. e.; Guldi, D. M. *C. R. Chimie* **2006**, *9*, 892–908. (e) Langford, S. J.; Latter, M. J.; Woodward, C. P. *Photochem. Photobiol.* **2006**, *82*, 1530–1540. (f) Prodi, A.; Chiorboli, C.; Scandola, F.; Lengo, E.; Alessio, E.; Dobrawa, R.; Würthner, F. *J. Am. Chem. Soc.* **2005**, *127*, 1454–1562.

(7) (a) Imahori, H.; Fukuzumi, S. *Adv. Funct. Mater.* **2004**, *14*, 525–536. (b) Imahori, H.; Mori, Y.; Matano, Y. *J. Photochem. Photobiol., C* **2003**, *4*, 51–83. (c) Gust, D.; Moore, T. A.; Moore, A. L. *Acc. Chem. Res.* **2001**, *34*, 40–48. (d) Armaroli, N.; Marconi, G.; Echegoyen, L.; Bourgeois, J.-P.; Diederich, F. *Chem.—Eur. J.* **2000**, *6*, 1629–1645. (e) Kurreck, H.; Huber, M. *Angew. Chem., Int. Ed. Engl.* **1995**, *34*, 849–866.

(8) (a) Kadish, K. M.; Caemelbecke, V.; Royal, G. In *The Porphyrin Handbook*; Kadish, K. M., Smith, K. M., Guilard, R., Eds.; Academic Press: San Diego, CA, 2000; Vol. 8, pp 1−114. (b) Fukuzumi, S. In *The Porphyrin Handbook*; Kadish, K. M., Smith, K. M., Guilard, R., Eds.; Academic Press: San Diego, CA, 2000; Vol. 8, pp 115−151.

(9) (a) *Phthalocyanines: Properties and Applications*; Leznoff, C. C., Lever, A. B. P., Eds.; VCH: Weinheim, Germany, 1989, 1993, 1996; Vols. 1−4. (b) Hanack, M.; Heckmann, H.; Polley, R. In *Methods in Organic Chemistry (Houben-Weyl)*; Schaumann, E., Ed.; Thieme: Stuttgart, Germany, 1998; Vol. E 9d, p 717. (c) de la Torre, G.; Nicolau, M.; Torres, T. In *Phthalocyanines: Synthesis, Supramolecular Organization and Physical Properties in Supramolecular Photosensitive and Electroactive Materials*; Nalwa, H. S., Ed.; Academic Press: New York, 2001. (d) *The Porphyrin Handbook*; Kadish, K. M., Smith, K. M., Guilard, R., Eds.; Academic Press: San Diego, CA, 2003; Vols. 15−20. (e) de la Torre, G.; Vázquez, P.; Agulló-López, F.; Torres, T. *Chem. Rev.* **2004**, *104*, 3723–3750. (f) Chen, Y.; El-Khouly, M. E.; Doyle, J. J.; Lin, Y.; Liu, Y.; Notaras, E. G. A.; Blau, W. J.; O'Flaherty, S. M. Phthalocyanines and Related Compounds: Nonlinear Optical Response and Photoinduced Electron Transfer Process. *Handbook of Organic Electronics and Photonics*; Nalwa, H. S. Ed.; American Scientific Publishers, Stevenson Ranch, CA, 2008; Vol. 2, pp 151−181.

(10) (a) Claessens, C. G.; Hahn, U.; Torres, T. *Chem. Rec.* **2008**, *8*, 75–97. (b) Reddy, P. Y.; Giribabu, L.; Lyness, C.; Snaith, H. J.; Vijaykumar, C.; Chandrasekharam, M.; Lakshmikantam, M.; Yum, J.-H.; Kalyanasundaram, K.; Grätzel, M.; Nazeeruddin, M. K. *Angew. Chem., Int. Ed.* **2007**, *46*, 373–376. (c) O'Regan, B. C.; Lopez-Duarte, I.; Martinez-Diaz, M. V.; Forneli, A.; Albero, J.; Morandeira, A.; Palomares, E.; Torres, T.; Durrant, J. R. *J. Am. Chem. Soc.* **2008**, *130*, 2906–2907. (d) Cid, J.-J.; Yum, J.-H.; Jang, S.-R.; Nazeeruddin, M. K.; Martinez-Ferrero, E.; Palomares, E.; Ko, J.; Graetzel, M.; Torres, T. *Angew. Chem., Int. Ed.* **2007**, *46*, 8358–8362. (e) Troshin, P. A.; Knoeppe, R.; Peregudov, A. S.; Peregudova, S. M.; Egginger, M.; Lyubovskaya, R. N.; Saricifti, N. S. *Chem. Mater.* **2007**, *19*, 5363–5372. (f) de la Torre, G.; Claessens, C. G.; Torres, T. *Chem. Commun.* **2007**, 2000–2015.

(11) Rio, Y.; Rodríguez-Morgade, M. S.; Torres, T. *Org. Biomol. Chem.* **2008**, *6*, 1877–1894, and references therein.

(12) (a) Maya, E. M.; García-Frutos, E. M.; Vázquez, P.; Torres, T.; Martín, G.; Rojo, G.; Agulló-Lopez, F.; González-Jonte, R. H.; Ferro, V. R.; García de la Vega, J. M.; Ledoux, I.; Zyss, J. *J. Phys. Chem. A* **2003**, *107*, 2110–2117. (b) Maya, E. M.; García, C.; García-Frutos, E. M.; Vázquez, P.; Torres, T. *J. Org. Chem.* **2000**, *65*, 2733–2739. (c) Maya, E. M.; Vázquez, P.; Torres, T. *Chem.—Eur. J.* **1999**, *5*, 2004–2013. (d) Gouloumis, A.; Liu, S. G.; Sastre, A.; Vázquez, P.; Echegoyen, L.; Torres, T. *Chem.—Eur. J.* **2000**, *6*, 3600–3607. (e) Guldi, D. M.; Gouloumis, A.; Vázquez, P.; Torres, T. *Chem. Commun.* **2002**, 2056–2057.

(13) (a) Guldi, D. M.; Ramey, J.; Martínez-Díaz, M. V.; de la Escosura, A.; Torres, T.; Da Ros, T.; Prato, M. *Chem. Commun.* **2002**, 2774–2775. (b) Martínez-Díaz, M. V.; Fender, N. S.; Rodríguez-Morgade, M. S.; Gómez-López, M.; Diederich, F.; Echegoyen, L.; Stoddart, J. F.; Torres, T. *J. Mater. Chem.* **2002**, *12*, 2095–2099. (c) Guldi, D. M.; Zilbermann, I.; Gouloumis, A.; Vázquez, P.; Torres, T. *J. Phys. Chem. B* **2004**, *108*, 18485–18494. (d) Li, X.; Sinks, L. E.; Rybtchinski, B.; Wasielewski, M. R. *J. Am. Chem. Soc.* **2004**, *126*, 10810–10811. (e) Rodríguez-Morgade, M. S.; Torres, T.; Atienza Castellanos, C.; Guldi, D. M. *J. Am. Chem. Soc.* **2006**, *128*, 15145–15154.

(14) (a) Jimenez, A. J.; Spänig, F.; Rodriguez-Morgade, M. S.; Ohkubo, K.; Fukuzumi, S.; Guldi, D. M.; Torres, T. *Org. Lett.* **2007**, *9*, 2481–2484. (b) Fukuzumi, S.; Ohkubo, K.; Ortiz, J.; Gutierrez, A. M.; Fernandez-Lazaro, F.; Sastre-Santos, A. *Chem. Commun.* **2005**, *30*, 3814–3816. (c) Norton, J. E.; Bredas, J.-L. *J. Chem. Phys.* **2008**, *128*, 034701/1–034701/7. (d) Tant, J.; et al. *J. Phys. Chem. B* **2005**, *109*, 20315–20323.

(15) (a) González-Cabello, A.; Vázquez, P.; Torres, T. *Tetrahedron Lett.* **1999**, *40*, 3263–3266. (b) Gouloumis, A.; Liu, S.-G.; Vázquez, P.; Echegoyen, L.; Torres, T. *Chem. Commun.* **2001**, 399–400. (c) González-Cabello, A.; Vázquez, P.; Torres, T.; Guldi, D. M. *J. Org. Chem.* **2003**, *68*, 8635–8642. (d) González-Rodríguez, D.; Claessens, C. G.; Torres, T.; Liu, S.; Echegoyen, L.; Vila, N.; Nonell, S. *Chem.—Eur. J.* **2005**, *11*, 3881–3893. (e) Campidelli, S.; Ballesteros, B.; Filoramo, A.; Diaz Diaz, D.; de la Torre, G.; Torres, T.; Rahman, G. M. A.; Ehli, C.; Kiessling, D.; Werner, F.; Sgobba, V.; Guldi, D. M.; Cioffi, C.; Prato, M.; Bourgoin, J.-P. *J. Am. Chem. Soc.* **2008**, *130*, 11503–11509.

fullerene conjugates[12d,e,13c,17,18] and supramolecularly assembled phthalocyanine−fullerene hybrids[13a,b,19,20] displaying long-lived charge-separated states ranging from a few nanoseconds[12e] to milliseconds.[17d]

It has been confirmed in numerous studies, including ours,[17−19] that small variations in the assembling mode of the donor and acceptor components can have an effect on the charge-separated state lifetime, this being as important in many cases as the choice of the electroactive units. The use of supramolecular interactions has proven to be a useful and efficient strategy to access some architectures, which are otherwise more difficult to access or even inaccessible by covalent chemistry. In particular, coordination to the central metal of the macrocycles by ligands containing the fullerene unit is an excellent method to produce complex photoactive arrays from simple building blocks.[21] Along these lines, we have prepared and studied the photophysics of the linear *N*-(4-pyridyl)-3,4-fulleropyrrolidine ligand (**1**; Chart 1), specifically designed to exhibit direct electronic coupling between the pyridyl nitrogen and the fullerene.[22] Unlike the related *N*-methyl-2-(4-pyridyl)pyrrolidine spacer, upon complexation with zinc(II) tetraphenylporphyrin, the *N*-(4-pyridyl)-pyrrolidine moiety proved to be an excellent bridge, providing electronic interaction between the porphyrin and the C_{60}.[22] In addition, we have recently reported a synthetic strategy for the selective preparation of fullerene−*trans*-1-bispyrrolidine adducts in moderate yields, by 1,3-dipolar cycloaddition of the readily accessible fullerene tetramalonate with suitable glycine derivatives.[23] We have now prepared a *trans*-1-bis[*N*-(4-pyridyl)fulleropyrrolidine] ligand (**2**; Chart 1) by following a similar synthetic protocol.

Chart 1. Structures of the Fullerene Monopyridyl and Bispyridyl Ligands [C_{60}Py] (**1**) and [$C_{60}Py_2$] (**2**)[a]

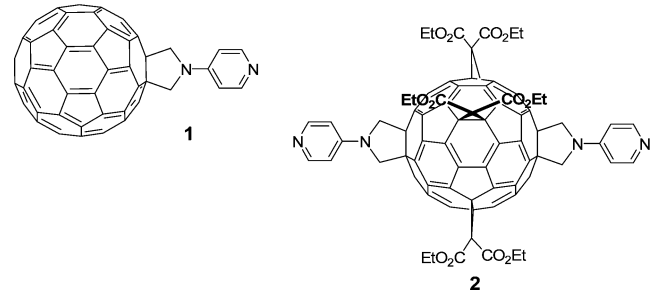

[a] The fourth malonate group of **2** has been omitted for clarity.

Owing to the simplicity of metal coordination as a synthetic approach to assemble metallomacrocycles and fullerene units, we presumed that it should also be relatively easy to study the effect of the donor−acceptor stoichiometry in the radical ion pair state lifetime, by selecting appropriate central metal ions and metallic phthalocyanine building blocks. Therefore, in this paper we report the convergent synthesis, electrochemical characterization, and photophysical studies of phthalocyanine−fullerene hybrids **3**−**5** bearing an orthogonal geometry (Chart 2) that have been assembled through metal coordination of linear fullerene mono- and bispyridyl ligands to ruthenium(II) phthalocyanines. The use of this convergent synthetic procedure allows to determine the influence of the donor and acceptor ratio on the radical ion pair state lifetime.

Results and Discussion

Synthesis of Phthalocyanine and Fullerene Building Blocks and Models. The phthalocyanine ligands were endowed with four *tert*-butyl substituents at their periphery since this kind of functionalization usually provides the desired solubility in organic solvents and reduces aggregation, without significantly altering the electron donor features of the phthalocyanine backbone.[24] Besides, ruthenium(II) phthalocyanines were selected among other types of metallophthalocyanines because the use of these complexes allows control of the geometry and stoichiometry of the arrays. We and others have used this kind of metallomacrocycle to arrange stable and rigid architectures through metal coordination of pyridine derivatives.[25] Thus, single ligation at the Ru(II) ion of the phthalocyanine is guaranteed by placing the strongly ligating, π-acceptor carbonyl

(16) (a) Fukuzumi S.; Imahori, H. In *Electron Transfer in Chemistry*; Balzani, V., Ed.; Wiley-VCH: Weinheim, Germany, 2001; Vol. 2, pp 927−975. (b) Fukuzumi S.; Guldi, D. M. In *Electron Transfer in Chemistry*; Balzani, V., Ed.; Wiley-VCH: Weinheim, Germany, 2001; Vol. 2, pp 270−337. (c) Guldi, D. M.; Fukuzumi, S. In *Fullerenes: From Synthesis to Optoelectronic Properties*; Guldi, D. M., Martin, N., Eds.; Kluwer: Dordrecht, The Netherlands, 2003; pp 237−265.

(17) (a) Sastre, A.; Gouloumis, A.; Vázquez, P.; Torres, T.; Doan, V.; Schwartz, B. J.; Wudl, F.; Echegoyen, L.; Rivera, J. *Org. Lett.* **1999**, *1*, 1807–1810. (b) González-Rodríguez, D.; Torres, T. In *The Exciting World of Nanocages and Nanotubes*, Proceedings of the Electrochemical Society, Fullerenes; Kamat, P., Guldi, D. M., Kadish, K., Eds.; Electrochemical Society: Pennington, NJ, 2002; Vol. 12, pp 195−210. (c) Loi, M. A.; Neugebauer, H.; Denk, P.; Brabec, C. J.; Sariciftci, N. S.; Gouloumis, A.; Vázquez, P.; Torres, T. *J. Mater. Chem.* **2003**, *13*, 700–704. (d) Guldi, D. M.; Gouloumis, A.; Vázquez, P.; Torres, T.; Georgakilas, V.; Prato, M. *J. Am. Chem. Soc.* **2005**, *127*, 5811–5813.

(18) (a) Gouloumis, A.; de la Escosura, A.; Vazquez, P.; Torres, T.; Kahnt, A.; Guldi, D. M.; Neugebauer, H.; Winder, C.; Drees, M.; Sariciftci, N. S. *Org. Lett.* **2006**, *8*, 5187–5190. (b) Kahnt, A.; Guldi, D. M.; de la Escosura, A.; Martinez-Diaz, M. V.; Torres, T. *J. Mater. Chem.* **2008**, *18*, 77–82. (c) Quintiliani, M.; Kahnt, A. l.; Vazquez, P.; Guldi, D. M.; Torres, T. *J. Mater. Chem.* **2008**, *18*, 1542–1546. (d) Kahnt, A.; Quintiliani, M.; Vazquez, P.; Guldi, D. M.; Torres, T. *ChemSusChem* **2008**, *1*, 97–102. (e) Quintiliani, M.; Kahnt, A.; Woeffle, T.; Hieringer, W.; Vazquez, P.; Goerling, A.; Guldi, D. M.; Torres, T. *Chem.−Eur. J.* **2008**, *14*, 3765–3775.

(19) (a) Doyle, J. J.; Ballesteros, B.; de la Torre, G.; Torres, T.; Blau, W. J. *Chem. Phys. Lett.* **2006**, *428*, 307–311. Ballesteros, B.; de la Torre, G.; Torres, T.; Hug, G. L.; Rahmanc, G. M. A.; Guldi, D. M. *Tetrahedron* **2006**, *62*, 2097–2101. (b) Sessler, J. L.; Jayawickramarajah, J.; Gouloumis, A.; Dan Pantos, G.; Torres, T.; Guldi, D. M. *Tetrahedron* **2006**, *62*, 2123–2131. (c) de la Escosura, A.; Martinez-Diaz, M. V.; Guldi, D. M.; Torres, T. *J. Am. Chem. Soc.* **2006**, *128*, 4112–4118. (d) de la Escosura, A.; Martinez-Diaz, M. V.; Torres, T.; Grubbs, R. H.; Guldi, D. M.; Neugebauer, H.; Winder, C.; Drees, M.; Sariciftci, N. S. *Chem. Asian J.* **2006**, *1*, 148–154.

(20) For some examples of Pc−C_{60} assemblies reported by other research groups see: (a) Linssen, T. G.; Durr, K.; Hanack, M.; Hirsch, A. *J. Chem. Soc., Chem. Commun.* **1995**, *10*, 3–104. (b) Durr, K.; Fiedler, S.; Linssen, T.; Hirsch, A.; Hanack, M. *Chem. Ber.* **1997**, *130*, 1375–1378. (c) Tian, Z.; He, C.; Liu, C.; Yang, W.; Yao, J.; Nie, Y.; Gong, Q.; Liu, Y. *Mater. Chem. Phys.* **2005**, *94*, 444–448. (d) Kim, K. N.; Choi, C. S.; Kay, K.-Y. *Tetrahedron Lett.* **2005**, *46*, 6791–6795. Chen, Y.; El-Khouly, M. E.; Sasaki, M.; Araki, Y.; Ito, O. *Org. Lett.* **2005**, *7*, 1613–1616. (e) El-Khouly, M. E.; Kang, E. S.; Kay, K.-Y.; Choi, C. S.; Aaraki, Y.; Ito, O. *Chem.−Eur. J.* **2007**, *13*, 2854–2863.

(21) (a) Mateo-Alonso, A.; Sooambar, C.; Prato, M. C. R. *Chimie* **2006**, *9*, 944–951. (b) D'Souza, F.; Ito, O. *Coord. Chem. Rev.* **2005**, *249*, 1410–1422. (c) El-Khouly, M. E.; Ito, O.; Smith, P. M.; D'Souza, F. *J. Photochem. Photobiol., C* **2004**, *5*, 79–104.

(22) (a) Tat, F. T.; Zhou, Z.; MacMahon, S.; Song, F.; Rheingold, A. L.; Echegoyen, L.; Schuster, D. I.; Wilson, S. R. *J. Org. Chem.* **2004**, *69*, 4602–4606. (b) Wilson, S. R.; MacMahon, S.; Tat, F. T.; Jarowski, P. D.; Schuster, D. I. *Chem. Commun.* **2003**, *2*, 226–227. (c) Regev, A.; Galili, T.; Levanon, H.; Schuster, D. I. *J. Phys. Chem. A* **2006**, *110*, 8593–8598.

(23) Zhang, S.; Lukoyanova, O.; Echegoyen, L. *Chem.−Eur. J.* **2006**, *12*, 2846–2853.

(24) Li, R.; Zhang, X.; Zhu, P.; Ng, D. K. P.; Kobayashi, N.; Jiang, J. *Inorg. Chem.* **2006**, *45*, 2327–2334.

Chart 2. Structures of the Pc−C_{60} Hybrids [Ru(CO)(C_{60}Py)Pc] (**3**), [Ru(C_{60}Py)$_2$Pc] (**4**), and [Ru$_2$(CO)$_2$(C_{60}Py$_2$)Pc$_2$] (**5**)[a]

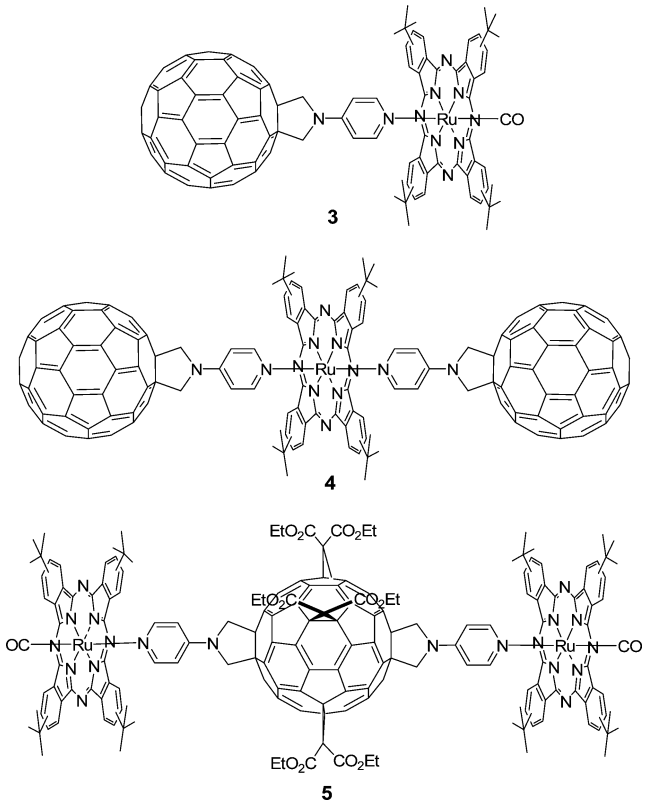

[a] The fourth malonate of **5** has been omitted for clarity.

ligand at one of the two axial Ru(II) coordination sites. This directs the other ligand, in this case the fulleropyridyl derivatives **1** and **2**, to the opposite phthalocyanine axial coordination site.[13e,26] On the other hand, phthalocyanines bearing two pyridyl axial ligands can be obtained under mild conditions from ruthenium(II) phthalocyanine precursors possessing the two axial coordination sites occupied by more labile ligands, such as nitrile derivatives.[10c,25−27]

The ruthenium carbonyl phthalocyanine precursor **6** was obtained in very good yield by the reaction of the corresponding phthalocyanine free base with trisruthenium dodecacarbonyl in phenol at reflux temperature, following a reported procedure.[13e] Irradiation of **6** in acetonitrile at room temperature for 15 min quantitatively afforded the bis(acetonitrile)ruthenium phthalocyanine (**7**; Scheme 1). Compound **7**, bearing two acetonitrile ligands on the axial phthalocyanine positions, is stable enough to be purified by column chromatography on silica gel. However, the Ru(II)−nitrile complexes show sufficient lability to be readily substituted by the stronger pyridyl ligands, so compound **7** was used as an intermediate in the synthesis of phthalocyanine

Scheme 1. Synthesis of Phthalocyanine Precursor **7** and Model Compounds **8** and **9**

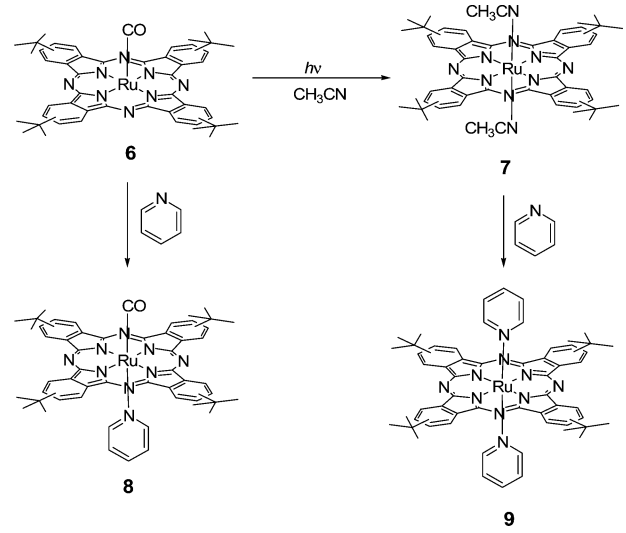

bispyridyl-based complexes, as we describe below. The model compound [Ru(CO)PyPc] (**8**)[28] was prepared by treating **6** with neat pyridine for 15 min (Scheme 1), while [RuPy$_2$Pc] (**9**) was obtained following the reported procedure.[27] Alternatively, compound **9** could be synthesized from **7** by treatment with neat pyridine, as represented in Scheme 1 (61% overall yield related to *tert*-butylphthalocyanine free base). Therefore, despite using three steps in the latter case, this synthetic procedure is more advantageous in terms of yield than a two-step method reported previously (34% overall yield related to the same precursor).[27]

The most remarkable spectroscopic feature of phthalocyanine **7** is the chemical shift assigned to the methyl protons corresponding to the acetonitrile ligands, which are strongly influenced by the phthalocyanine diatropic ring current and appear at $\delta = -0.17$ ppm. Likewise, model compound **8** displayed upfield-shifted signals at $\delta = 6.13$, 5.30, and 2.04 ppm, corresponding to the H$^{4'}$, H$^{3'}$ (and H$^{5'}$), and H$^{2'}$ (and H$^{6'}$) pyridyl protons, respectively. In addition, the IR spectrum of this compound was dominated by an intense band at 1969 cm^{-1}, assigned to the carbonyl ligand.

N-(4-Pyridyl)-3,4-fulleropyrrolidine ligand (**1**) was synthesized as previously reported.[22] The hexakis-substituted *trans*-1 ligand **2** was prepared via a protection−deprotection approach utilizing the concept of orthogonal transposition as outlined by Kräutler.[23,29] The advanced intermediate which became our starting material was the all-equatorial C_{60}-tetramalonate (**10**; Scheme 2), which was prepared as described previously.[23,29] Using **10** as the starting material, we then set about adding the pyridylpyrrolidine groups onto the fullerene via 1,3-dipolar cycloaddition reactions. We expected to cleanly add the pyridylpyrrolidine group by treating **10** with pyridylglycine[30] and paraformaldehyde. However, what we observed instead were two products which coeluted chromatographically. Through careful analysis of the ^{1}H NMR spectrum, and in particular the aromatic region, it was determined that a mixture of penta-adduct **13** and penta-adduct **14** was obtained in an approximately

(25) (a) Rawling, T.; Xiao, H.; Lee, S.-T.; Colbran, S. B.; McDonagh, A. M. *Inorg. Chem.* **2007**, *46*, 2805–2813. (b) Rawling, T.; McDonagh, A. M. *Coord. Chem. Rev.* **2007**, *251*, 1128–1157. (c) Mak, C. C.; Bampos, N.; Darling, S. L.; Montalti, M.; Prodi, L.; Sanders, J. K. M. *J. Org. Chem.* **2001**, *66*, 4476–4486. (d) Webb, S. J.; Sanders, J. K. M. *Inorg. Chem.* **2000**, *39*, 5912–5919.

(26) (a) Cammidge, A. N.; Berber, G.; Chambrier, I.; Hough, P. W.; Cook, M. J. *Tetrahedron* **2005**, *61*, 4067–4074. (b) Berber, G.; Cammidge, A. N.; Chambrier, I.; Cook, M. J.; Hough, P. W. *Tetrahedron Lett.* **2003**, *44*, 5527–5529.

(27) Rodríguez-Morgade, M. S.; Planells, M.; Torres, T.; Ballester, P.; Palomares, E. *J. Mater. Chem.* **2008**, *18*, 176–181.

(28) Ishii, K.; Shiine, M.; Shimizu, Y.; Hoshino, S.-i.; Abe, H.; Sogawa, K.; Kobayashi, N. *J. Phys. Chem. B* **2008**, *112*, 3138–3143.

(29) Schwenninger, R.; Müller, T.; Kraeutler, B. *J. Am. Chem. Soc.* **1997**, *119*, 9317–9318.

(30) Ohta, M.; Masaki, M. *Bull. Chem. Soc. Jpn.* **1960**, *33*, 1150.

Scheme 2. Synthesis of Bispyridyl Ligand [$C_{60}Py_2$] (**2**) (R = CO_2Et)[a]

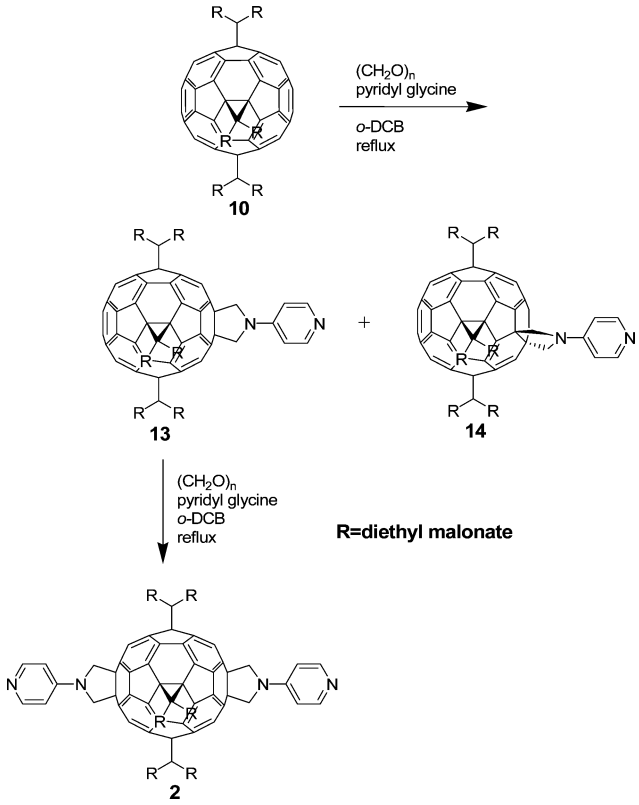

[a] The fourth malonate group of **2** has been omitted for clarity.

1:1 ratio (on the basis of the integration of the aromatic signals). Eventually, the two adducts were separated by careful column chromatography on silica gel using gravity instead of air pressure. In this way, pure **13** was obtained in 25% yield from **10**. Compound **13** was used in a second 1,3-dipolar cycloaddition reaction using conditions identical to those described above to give, after chromatographic separation, the hexakis-substituted *trans*-1 ligand **2** in 9% yield based on **13** (Scheme 2).

We are confident in our assignment of **2** as the *trans*-1 adduct based on the high symmetry shown in the ^{1}H NMR spectrum (see the Supporting Information). The most notable feature is a singlet for the eight equivalent pyrrolidine ring protons at $\delta =$ 4.88 ppm. Additionally, the two doublets in the aromatic region, as well as two well-defined quartets and two triplets, arising from the two magnetically inequivalent ethyl groups of the equatorial malonates, support the assignment of this compound as the *trans*-1 isomer.

Synthesis and Characterization of Phthalocyanine−Fullerene Hybrids 3−5. The hybrid [Ru(CO)(C_{60}Py)Pc] (**3**) was assembled by treatment of the phthalocyanine **6** and the *N*-(4-pyridyl)-3,4-fulleropyrrolidine ligand (**1**) in a 1:1 stoichiometric ratio in toluene at room temperature. The purification of **3** was done by gel permeation chromatography (Biobeads SX-3, toluene), affording the dyad in 80% yield. Likewise, the triad [$Ru_2(CO)_2(C_{60}Py_2)Pc_2$] (**5**) was prepared in 65% yield by stirring the phthalocyanine **6** and the corresponding fullerene−bispyridyl ligand **2** in a 2:1 stoichiometric ratio, respectively. In this case, chloroform was used as the reaction solvent, because of the enhanced solubility of the fullerene building block **2** in organic solvents, as a result of the tetramalonate functionalization. The triad [Ru($C_{60}Py)_2$Pc] (**4**) was obtained in a similar manner by heating a 2:1 mixture of **1** and the phthalocyanine precursor **7** in toluene at 60−80 °C. Purification by gel permeation chromatography (Biobeads SX-3, toluene) gave the complex in 58% yield.

The chemical characterization of the phthalocyanine−fullerene hybrids **3**−**5** was carried out by ^{1}H and ^{13}C NMR, UV/vis, and IR spectroscopies, as well as mass spectrometry. The three compounds displayed the orthogonal geometry of the two electroactive units. As a consequence, the fullerene moiety experiences the influence of the phthalocyanine ring current in the shielding cone. Hence, ^{1}H NMR spectroscopy provided a quite useful and unequivocal tool to characterize these compounds, on the basis of their expected, characteristic, high-field shifted signals, corresponding to the fullerene−pyridyl and −pyrrolidine moieties. The array **3** showed the two pyridyl signals at $\delta = 4.95$ ($H^{3'}$, $H^{5'}$) and 1.85 ($H^{2'}$, $H^{6'}$) ppm, the latter considerably more shielded due to the proximity of these protons to the phthalocyanine aromatic core, while the more distant pyrrolidine protons appeared at $\delta = 4.23$ ppm (0.77 ppm shielded relative to the precursor, Figure 1).[22] Remarkably, the shielding effect of the phthalocyanine ring current on the fulleropyrrolidine moiety is even more evident for triad **5**. In this case, due to the presence of two phthalocyanine macrocycles, the signals corresponding to the pyridyl protons appear at $\delta = 4.58$ and 1.70 ppm, with the pyrroline protons shifted upfield by 1.5 ppm relative to the fullerene bispyridyl precursor **2** (Figure 1). The triad **4** showed two pyridyl-type protons at $\delta = 4.99$ and 2.51 ppm, somewhat less shifted than in **3** and **5**.

The MS spectrum of complex **4** (MALDI-TOF, dithranol) exhibits the isotopic clusters corresponding to the two molecular components at $m/z = 832-842$ ($[RuPc]^+$) and 840 ($[C_{60}Py]^+$), in addition to the most intense peak at $m/z = 1668-1684$, which always appears for this type of phthalocyanine, due to the RuPc dimer. It was also possible to detect the molecular ion $[M]^+$ as a weaker peak at $m/z = 2512-2525$ (see the Supporting Information). The corresponding molecular ion $[M]^+$ for dyad **3** was not detected by MS by any of the attempted techniques (MALDI-TOF, LSIMS, and ESI). Instead, a cluster at $m/z = 1677-1683$, assignable to $[M - CO]^+$, was observed, superimposed with the cluster matching the RuPc dimer (see the Supporting Information). The loss of the carbonyl ligand under these mass spectrometric conditions has previously been observed for similar compounds.[13e] The main peaks of the spectrum are again those corresponding to the molecular fragments at $m/z = 860-870$ and 832−842 ($[Ru(CO)Pc]^+$ and $[RuPc]^+$, respectively) and 840 ($[C_{60}Py]^+$). Compound **5** proved to be even more labile, and no ion which could be assigned to an assembled structure was detected. Instead, peaks corresponding to the molecular units at $m/z = 860-870$ and 832−842 ($[Ru(CO)Pc]^+$ and $[RuPc]^+$, respectively), 1668−1684 (RuPc dimer), and 1593 ($[C_{60}Py_2 + H]^+$) were detected (see the Supporting Information).

The attachment of a fulleropyrrolidine moiety to the pyridyl ligand does not severely alter the original weak σ-donor and π-acceptor features of pyridine. This is supported by the carbonyl stretching frequency displayed by compound **3**, which is identical to that of the corresponding model **8** and appears at $\nu = 1969$ cm^{-1}.[31] Compound **5** also displays an almost unaltered carbonyl stretching band at 1971 cm^{-1}, in addition to another intense band at 1740 cm^{-1}, which was assigned to the carboxyl moiety of the malonate substituents.

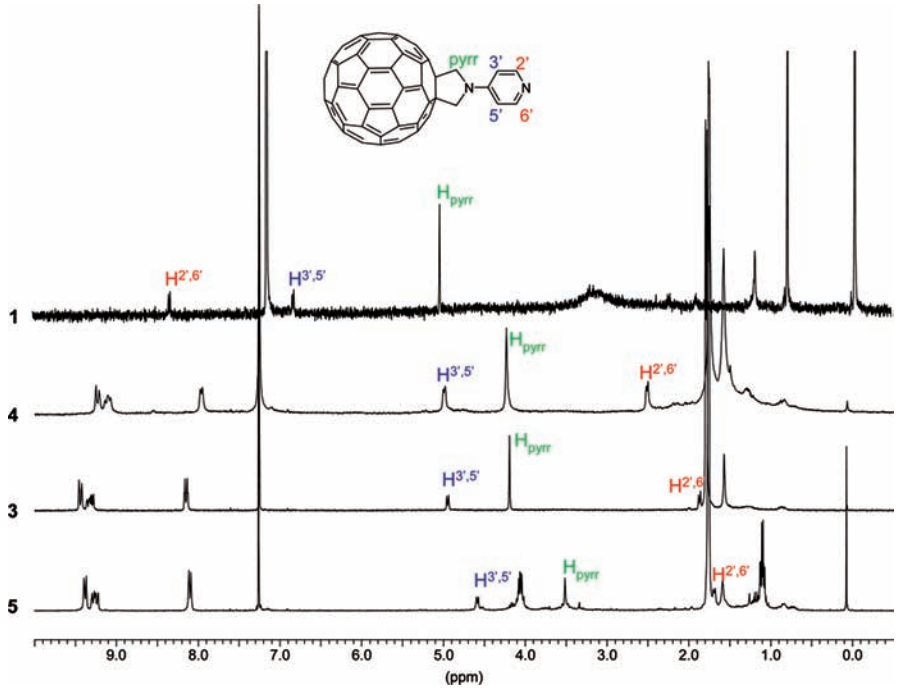

Figure 1. ^{1}H NMR spectra of ligand **1** in C_6D_6 vs complexes **3**, **4**, and **5** in $CDCl_3$.

Contrasting to what was observed for the reported ZnTPP−**1** complex,[22a] the UV/vis spectra of assemblies **3**−**5** correspond to that of the sum of their molecular parts in a stoichiometric ratio (Figures 2 and S18, Supporting Information). This is especially true for the phthalocyanine Q-band, which appears only 2 nm blue-shifted with respect to the references **6** and **9** in the same solvent. A similar tendency is observed for the three compounds **3**−**5** (see the Experimental Section). The high-energy region comprising the C_{60}, as well as the RuPc, charge transfer and Soret bands is more difficult to study in detail due to the superposition of these absorptions. Still, a careful analysis of the region shows small, but appreciable changes in the optical features of the C_{60} or Pc moiety. These differences are the following: (i) Compound **3** shows a hypsochromic shift of the fullerene band appearing at 333 nm in the model (Figure 2). (ii) Triad **4** exhibits considerable broadening in this region (Figure 2), and the Soret band at 318 nm, which would be expected to be similar to that of the Pc model **9**, appears 80% more intense in array **4**; this is the result of a blue shift of the 333 nm C_{60} absorption. (iii) Compound **5** (see the Supporting Information, Figure S18) also shows some broadening in the high-energy region of the spectrum, together with a bathochromic shift of the Soret band from 286 to 305 nm.

All of these observations suggest electronic coupling between the Pc moiety and the C_{60} unit in the ground state, which was further confirmed by electrochemical studies.

Electrochemical Studies. The electrochemical studies of arrays **3**−**5** and models **2**, **8**, and **9** were carried out using both cyclic voltammetry (CV) and differential pulse voltammetry (DPV) to probe electronic coupling between the two electroactive subunits. Figures S19 (Supporting Information) and 3 show the cyclic voltammograms and differential pulse voltammograms of the studied compounds, respectively. In addition, Tables 1 and S1 (Supporting Information) list the measured potentials determined by DPV and by CV (i.e., **1**−**5**, **8**, and **9**), respectively. Unless otherwise noted, the discussion is based on the DPV data. All redox processes corresponding to the ruthenium(II) phthalocyanine unit are ligand-based and not metal-based, in agreement with previous electrochemical studies carried out with similar metallomacrocycles.[25a,b]

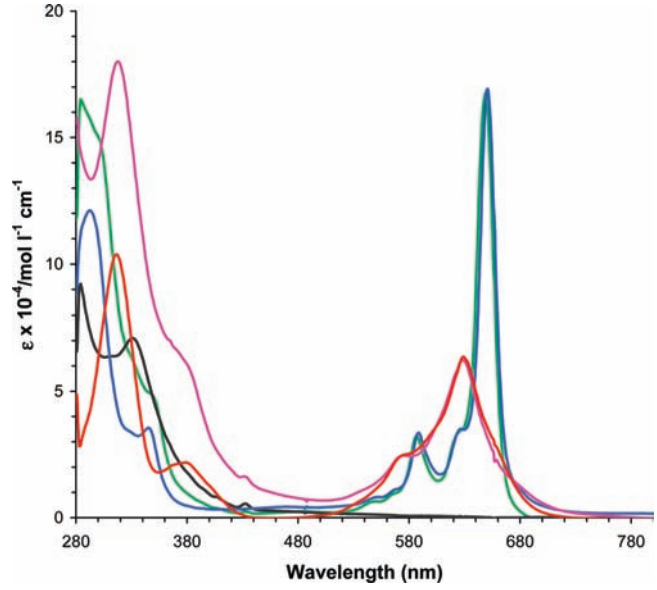

Figure 2. Comparison among UV/vis spectra of models **1** (black line), **6** (blue line), and **9** (red line) and their respective complexes **3** (green line) and **4** (pink line) in toluene.

(31) A σ-donor ligand increases the electron density in the metal center, thus allowing unimpeded metal to CO π-back-bonding. Moreover, a π-back-bonding ligand partially competes for the same metal d-orbital electron density, weakening the net M−CO π-back-bonding. These effects, in turn, have an influence on the ν(CO) IR stretching frequencies in metal carbonyl complexes, so that, as the electron density on a metal decreases, the M−C≡O resonance structure becomes more important and the ν(CO) IR stretching frequency increases. Likewise, as the electron density of the metal decreases, the M=C=O character becomes more important and the ν(CO) IR frequency decreases.

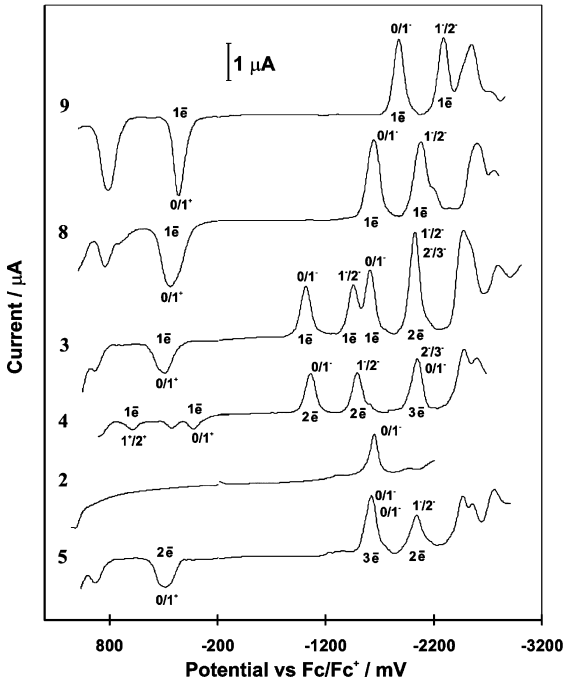

Figure 3. Differential pulse voltammograms recorded on a GC electrode (1 mm) in an acetonitrile/toluene (1:4, v/v) solvent mixture containing 0.1 mol L^{-1} (n-Bu)$_4$NPF$_6$ as the supporting electrolyte and 1.21×10^{-3} mol L^{-1} **9**, 1.28×10^{-3} mol L^{-1} **8**, 1.16×10^{-3} mol L^{-1} **3**, 1.15×10^{-3} mol L^{-1} **4**, 0.81×10^{-3} mol L^{-1} **2**, and 1.05×10^{-3} mol L^{-1} **5**. Parameters: pulse amplitude 0.05 V, pulse width 0.05 s, sampling width 0.017 s, pulse period 0.2 s.

The redox properties of hybrids **3**−**5** are different from those of the model complexes **1**, **2**, **8**, and **9**. The most pronounced difference results from the π-acceptor CO ligand—present in arrays **3** and **5**—on the complexes. When comparing the behaviors of **8** and **9**, the first reduction potential is shifted from −1.89 to −1.66 V (i.e., 230 mV shift), reflecting the strong accepting ability of the CO ligand. When comparing the reduction potentials of **8** and **3**, we note a further anodic shift of the potentials corresponding to the Pc moiety. The first Pc reduction is shifted by 40 mV, the second is shifted by 70 mV, and the third reduction is shifted by 130 mV. However, the C_{60}-centered reductions for **3** remain relatively constant as in model **1**. In addition, all oxidation potentials are shifted anodically—the first one by 80 mV and the second one by 90 mV.

When comparing the behavior of **5** and **8**, the first and second Pc-centered reductions are shifted anodically by 10 and 50 mV, respectively. The third reduction, which is also shifted anodically, splits into two processes at −2.48 and −2.57 V. As expected, the Pc-based oxidations are shifted to higher potentials. The first oxidation of **5** is shifted anodically by 30 mV with respect to the same process in **8**, while the second oxidation is shifted by 90 mV. The fact that the first oxidation peak of **5** involves both Pc units implies that there is a lack of appreciable electronic coupling between the two phthalocyanine moieties. A similar conclusion is derived from the reductive processes. In summary, Pc-centered oxidations and reductions in **3** and **5** are shifted anodically (easier to reduce and more difficult to oxidize), relative to the corresponding values of model **8**. As expected, the C_{60}-centered reductions are not very different from those for model **2**.

The introduction of two fulleropyrrolidines in **4** leads to a cathodically shifted reduction from −1.89 V in **9** to −2.05 V in **4** (160 mV shift, or 80 mV per pyrrolidine). The second reduction is also shifted cathodically by 220 mV, from −2.30 to −2.52 V. On the other hand, the C_{60}-based reductions remain essentially unchanged with respect to those for model compound **1**, and since they appear at the same potential for both C_{60} components, these subunits are not strongly coupled. Therefore, the following assignments can be made: the peaks at −1.06 V (2 e^- process) and at −1.47 V (2 e^-) correspond to C_{60}-centered processes, the peak at −2.05 V (3 e^-) corresponds to an overlap between C_{60}- and Pc-based reductions, and the peak at −2.52 V, as well as the smaller peak at the edge of the solvent potential window, correspond to Pc. The Pc ring is considerably more difficult to reduce when complexed to two fulleropyrrolidine ligands.

The anodic scans of **4** (CV and DPV) are notably different from those of the corresponding model **9**, as shown in Figures 3 and S19 (Supporting Information). While **9** revealed only two oxidation peaks, **4** exhibits three oxidation processes (Figures 3 and S19), although the current for the second process at +0.25 V (DPV) is much smaller than that of the other two processes at +0.05 and +0.60 V (see Figure S19). Additional work is currently under way to understand these two close oxidation processes. Another observed difference with respect to the other compounds is that the current of the oxidation peaks is considerably smaller than those of the reduction peaks. This has been attributed to an aggregation effect, which is known to produce a noticeable decrease of the intensity of the waves. Using the DPV results, the first oxidation of **9** is shifted cathodically from +0.17 to +0.05 V compared to that of **4**, while the last one is shifted from +0.83 to +0.60 V. The redox behavior of **4** reflects the electron-donating ability of the two *N*-(4-pyridyl)fulleropyrrolidine ligands, which results in an easier to oxidize and more difficult to reduce Pc center.[32] For complexes **3** and **5**, the electron-donating ability of the fulleropyrrolidine is somewhat balanced by the strong π-acceptor carbonyl ligands.

Photophysical Studies. The first part of the photophysical investigation was focused on determining the singlet-excited-state energies of the individual constituents (i.e., [Ru(CO)PyPc] (**8**), [RuPy$_2$Pc] (**9**), [C_{60}Py] (**1**), and [C_{60}Py$_2$] (**2**)) and on approximating intramolecular deactivation in the donor−acceptor hybrids (i.e., [Ru(CO)(C_{60}Py)Pc] (**3**), [Ru(C_{60}Py)$_2$Pc] (**4**), and [Ru$_2$(CO)$_2$(C_{60}Py$_2$)Pc$_2$] (**5**)) by means of fluorescence spectroscopy. **8**, **9**, **1**, and **2** fluoresce with maxima at 660, 655, 715, and 660 nm, respectively. Considering these short-wavelength emission maxima together with the long-wavelength absorption maxima at 650, 630, 690, and 630 nm, we estimate singlet-excited-state energies of 1.89, 1.92, 1.79, and 1.93 eV. Notable are the low fluorescence quantum yields that all the different constituents exhibit: **8** (3.7×10^{-5}), **9** (4.0×10^{-6}), **1** (6.0×10^{-4}), and **2** (2.5×10^{-3}). Despite the overall low quantum yields, the RuPc-centered emission is quenched in **3** and **4** by approximately a factor of 2, but remains nearly unquenched in **5**. The dominating RuPc absorption throughout the visible range rendered an investigation of the C_{60}-centered emission pointless.

In summary, the fluorescence experiments provided a first insight into the intramolecular charge transfer events that commence with the photoexcitation of RuPc. To shed light on the nature of the product, evolving from such intramolecular deactivations, complementary transient absorption measurements—ranging from femto- to microseconds—were conducted.

(32) Haas, M.; Liu, S.-X.; Kahnt, A.; Leiggener, C.; Guldi, D. M.; Hauser, A.; Decurtins, S. *J. Org. Chem.* **2007**, *72*, 7533–7543.

Table 1. Electrochemical Reduction and Oxidation Potentials, E_p, vs Fc/Fc^+ of **2**−**5**, **8**, and **9** and Free Energies of Charge Separation of **3**−**5**

	potential/V, E_p, vs Fc/Fc^+										
			reduction								
	oxidation		C_{60} base				Pc base				
compound	$E^{0/+}$	$E^{1+/2+}$	$E^{0/-}$	$E^{1-/2-}$	$E^{2-/3-}$	$E^{3-/4-}$	$E^{0/-}$	$E^{1-/2-}$	$E^{2-/3-}$	HOMO−LUMO gap[a]	$-\Delta G_{CS}^0$
9, [$RuPy_2Pc$]	+0.17	+0.83					−1.89	−2.30	−2.56		
8, [Ru(CO)PyPc]	+0.26	+0.86					−1.66	−2.1	−2.62		
3, [Ru(CO)(C_{60}Py)Pc]	+0.34	+0.95	−1.03	−1.47	−2.03[b]	−2.49[b]	−1.62	−2.03[b]	−2.49[b]	1.37	0.43[c]
4, [$Ru(C_{60}Py)_2Pc$]	+0.05 +0.25	+0.60	−1.06	−1.47	−2.05[b]	−2.52[b]	−2.05[b]	−2.52[b]		1.11	0.69[c]
2, [$C_{60}Py_2$]			−1.66								
5, [$Ru_2(CO)_2(C_{60}Py_2)Pc_2$]	+0.29	+0.95	−1.65[b]				−1.65[b]	−2.05	−2.48 −2.57	1.94	0.01[c]
1, [$C_{60}Py$][22a]			−1.06	−1.44	−1.93						

[a] Electrochemical HOMO−LUMO gap (eV): $\Delta E = E_{ox\,1} - E_{red\,1}$. [b] Reduction processes of the C_{60} and Pc bases overlap. [c] In toluene, exciting the C_{60} moiety.

We tested the individual constituents (i.e., **8**, **9**, **1**, and **2**) by means of transient absorption measurements. As an example, when **8** is photoexcited at 387 or 660 nm, the instantaneous population of the singlet excited state (1.89 eV) is observed to undergo differential absorption changes that include a series of maxima at 525, 700, 920, 1020, and 1150 nm. In **9** (1.92 eV), the maxima are shifted to 515, 705, and 950 nm. Minima, on the other hand, emerge at 650 or 630 nm as mirror images to the ground state. The **8** and **9** singlet-excited-state features are short-lived (10^{10} s^{-1}) and are converted—as indicated in Figure 4—via a rapid intersystem crossing to the energetically lower lying triplet-excited-state features (∼1.3 eV). A heavy atom effect is thought to be responsible for this intrinsic trend.[32]

Characteristics of the **8** triplet excited state are maxima at 520 and 730 nm that flank a minimum at 650 nm. In the case of **9**, the triplet-excited-state features are maxima at 520, 730, and 815 nm in addition to a minimum at 630 nm. Taking the intersystem crossing dynamics, we estimate singlet lifetimes of 6 ± 0.1 ps (1.6×10^{11} s^{-1}) and 3.6 ± 0.5 ps (2.7×10^{11} s^{-1}) for **8** and **9**, respectively. In the complementary recorded nanosecond spectra only the long-lived triplet-excited-state features are seen. Under anaerobic conditions the triplet lifetimes are on the order of 12 μs; however, when molecular oxygen is admitted, a nearly diffusion controlled deactivation results in cytotoxic singlet oxygen formation.

Transient absorptions of **1** and **2** are presented in Figure 5. In particular, when excited at 387 nm, we note a **1** singlet excited state (1.79 eV) that gives rise to a marked absorption around 920 nm. Once generated, this state is subject to a slow intersystem crossing process (7.4×10^8 s^{-1}) to yield the energetically lower lying triplet excited state (1.50 eV). This interconversion for **1** is nearly quantitative with a quantum yield of 0.98, due to a strong spin−orbit coupling as the modus operandi.[33] The correspondingly formed **1** triplet−triplet absorptions reveal maxima in the ultraviolet region (360 nm) and in the visible region (700 nm), which are susceptible to a reaction with molecular oxygen. In the absence of molecular oxygen the triplet lifetime is close to 20 μs. The photophysical features of this monoadduct are close to those of pristine C_{60}.

The functionalization pattern in **2**—a symmetrical hexakisadduct—results in a number of drastic changes in the electronic structure of C_{60}. In particular, the **2** singlet-excited-state (1.93 eV) features are shifted to the red with a long-wavelength maximum at 1050 nm. Despite the fact that the singlet lifetime

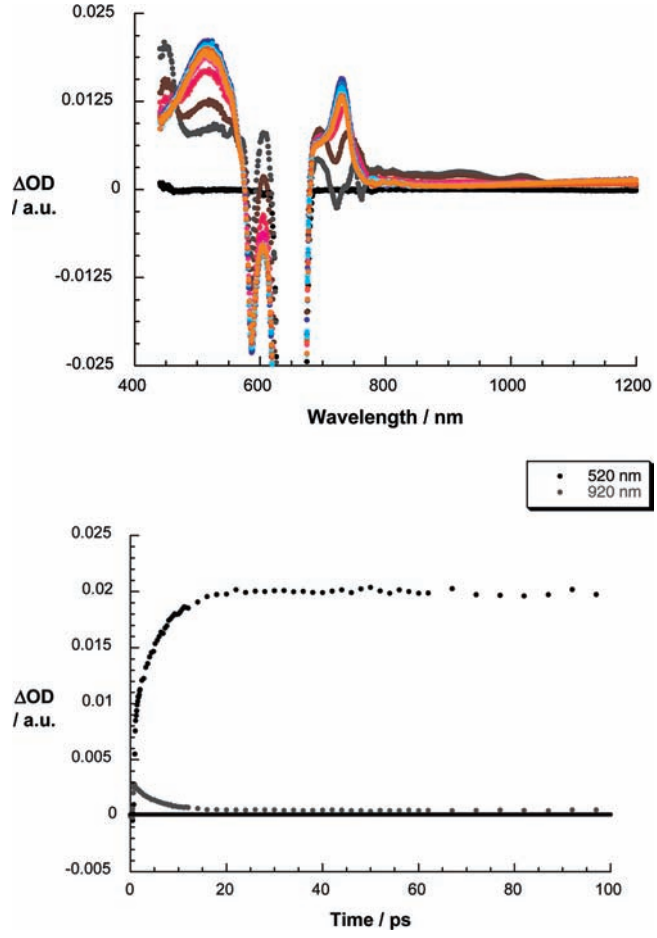

Figure 4. Top: differential absorption spectra (visible and near-infrared) obtained upon femtosecond flash photolysis (660; 150 nJ) of **8** in toluene (10 μM) with several time delays between 0 and 100 ps at room temperature. Bottom: time−absorption profile of the spectra shown above at 520 nm (black spectrum) and 920 nm (gray spectrum), reflecting intersystem crossing.

(6.0×10^8 s^{-1}) is close to that seen in **1**, the triplet quantum yield is only 0.15.[34]

Finally, the donor−acceptor hybrids (i.e., **3**, **4**, and **5**) were probed at 387 or at 660 nm to excite the C_{60} and RuPc constituents, respectively. Immediately, following the 387 nm laser excitation of **3**, **4**, and **5**, the strong singlet−singlet

(33) Martín, N.; Sánchez, L.; Illescas, B.; González, S.; Herranz, M. A.; Guldi, D. M. *Carbon* **2000**, *38*, 1577–1585.

(34) Not surprisingly, the characteristic [$C_{60}Py_2$] **2** triplet excited state is barely visible at 590 nm.

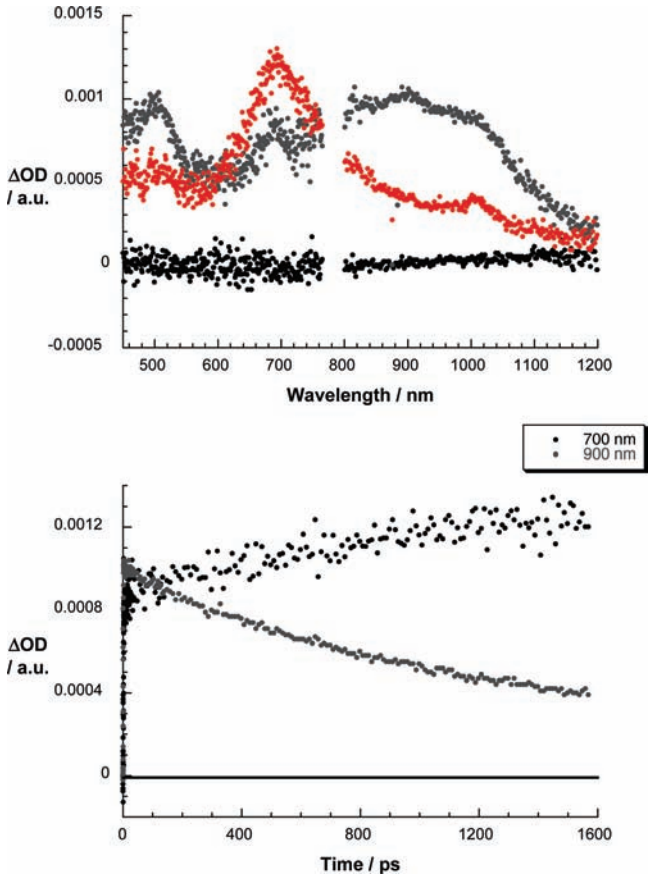

Figure 5. Top: differential absorption spectra (visible and near-infrared) obtained upon femtosecond flash photolysis (387; 150 nJ) of **1** in toluene (10 μM) with time delays of 0 ps (black spectrum), 5 ps (gray spectrum), and 3000 ps (red spectrum) at room temperature. Bottom: time−absorption profile of the spectra shown above at 700 nm (black spectrum) and 920 nm (gray spectrum), reflecting the intersystem crossing.

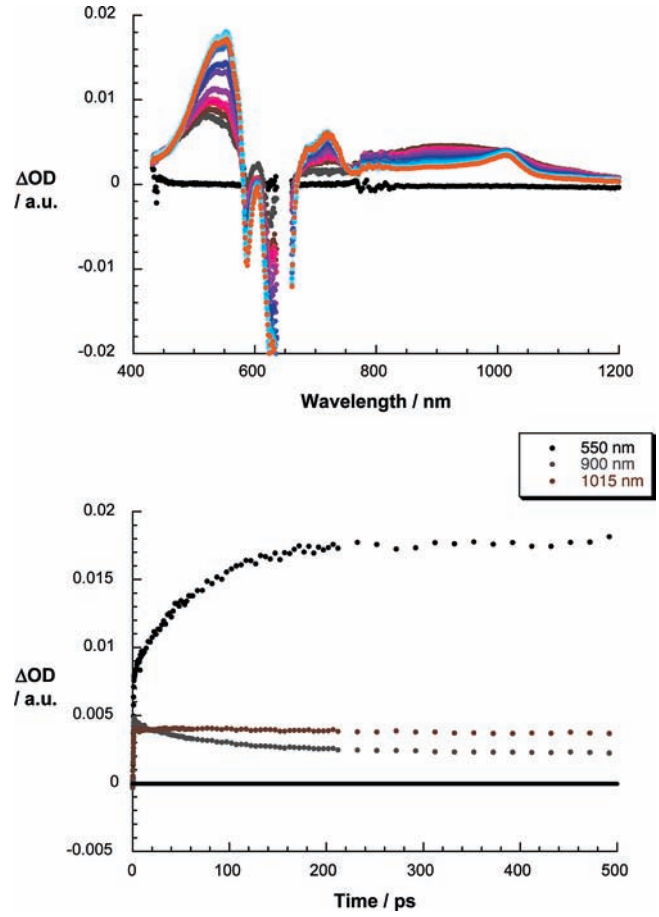

Figure 6. Top: differential absorption spectra (visible and near-infrared) obtained upon femtosecond flash photolysis (387; 150 nJ) of **3** in toluene (10 μM) with several time delays between 0 and 500 ps at room temperature. Bottom: time−absorption profile of the spectra shown above at 550 nm (black spectrum), 900 nm (gray spectrum), and 1015 nm (brown spectrum), reflecting the charge separation.

absorptions of C_{60} were registered at either 950 or 1050 nm—Figures 6 and 7. This confirms, despite the presence of one or two RuPc constituents, the successful formation of the **1** and **2** singlet excited states. However, instead of seeing the slow intersystem crossing dynamics, the singlet−singlet absorptions decay in the presence of one electron-donating RuPc constituent (i.e., **3** or **4**) or two electron-donating RuPc constituents (i.e., **5**) with accelerated dynamics. Concomitant with the C_{60} singlet-excited-state decay, new features develop in the visible and near-infrared regions. The transient absorption changes taken, for example, after the completion of the decay bear no resemblance with those of the C_{60} triplet excited state and/or of the RuPc triplet excited state. In the visible, the new transients for **3** (Figure 6) and **5** reveal strong maxima at 525/725 nm and minima at 585/660 nm.

For **4**, on the other hand, the new features include maxima at 535/715/885 nm and minima at 625 nm (Figure 7). In all of the cases the features match those of the one-electron-oxidized RuPc radical cations (i.e., models **8** and **9**).[13e] In the near-infrared range, on the other hand, the fingerprints of the one-electron-reduced C_{60} radical anion evolve at 1015 (i.e., model **1**) and 950 nm (i.e., **2**).[35] Moreover, changing the solvent polarity (i.e., toluene versus anisole) leads to an acceleration of the RuPc singlet-excited-state decay. All of these observations are well-rationalized when considering the free energy changes that are associated with an intramolecular charge transfer between the C_{60} singlet excited state—the electron acceptor—and the RuPc ground state—the electron donor—that afford the $C_{60}^{\bullet-}$/$RuPc^{\bullet+}$ radical ion pair states as sole products. From a multiwavelength analysis of the singlet-excited-state decay and the radical ion pair state growth, we have determined the following charge transfer rate constants in toluene/anisole: 1.5×10^{10} s^{-1}/1.0×10^{10} s^{-1} (**3**), 1.7×10^{10} s^{-1}/1.3×10^{10} s^{-1} (**4**), 1.8×10^{10} s^{-1}/2.0×10^{10} s^{-1} (**5**).

To supplement the aforementioned experiments, we turned to 660 nm excitation, which affects RuPc exclusively. In fact, detection of the instantaneously growing 1050 or 950 nm absorption confirms the RuPc excitation in **3**, **4**, and **5**. This is in excellent agreement with what has been observed with **8** and **9**. Similar to the 387 nm excitation, where the C_{60} singlet excited state is subject to an accelerated decay, the RuPc singlet excited state decays rapidly. For example, in toluene the lifetimes are 4.5 and 1.7 ps for **3** and **4**, respectively. Again, the fingerprints of the one-electron-oxidized RuPc radical cations and of the one-electron-reduced C_{60} radical anions are seen in the visible and near-infrared ranges, respectively. In **3** the growth dynamics of the $C_{60}^{\bullet-}$/$RuPc^{\bullet+}$ radical ion pair state (2.2×10^{11} s^{-1}) matches the dynamics of the singlet decay. On the other hand,

(35) Zhou, Z.; Sarova, G. H.; Zhang, S.; Ou, Z.; Tat, F. T.; Kadish, K. M.; Echegoyen, L.; Guldi, D. M.; Schuster, D. I.; Wilson, S. R. *Chem.—Eur. J.* **2006**, *12*, 4241–4148.

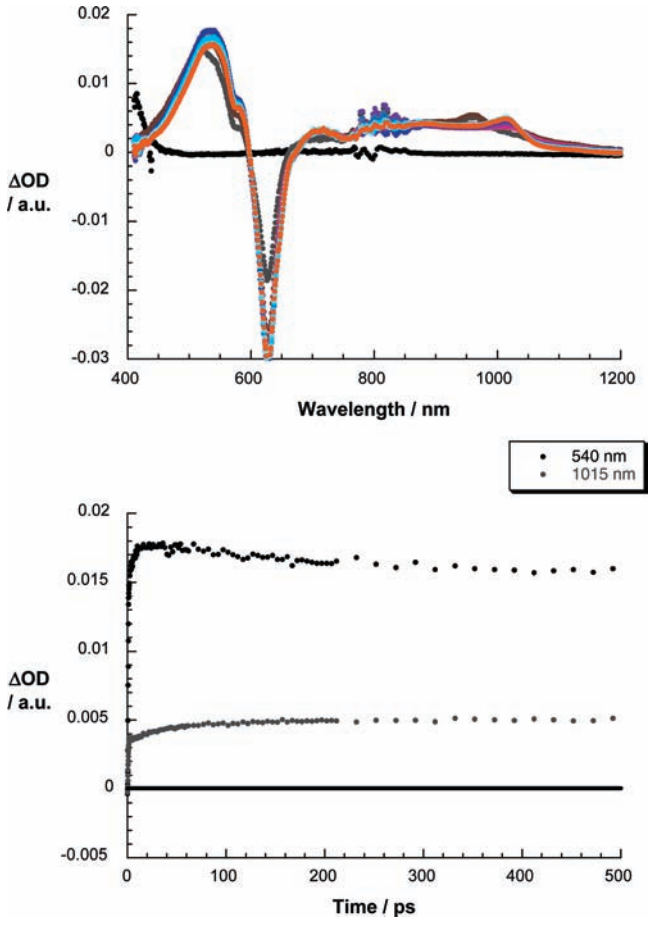

Figure 7. Top: differential absorption spectra (visible and near-infrared) obtained upon femtosecond flash photolysis (387; 150 nJ) of **4** in toluene (10 μM) with several time delays between 0 and 500 ps at room temperature. Bottom: time−absorption profile of the spectra shown above at 540 nm (black spectrum) and 1015 nm (gray spectrum), reflecting the charge separation.

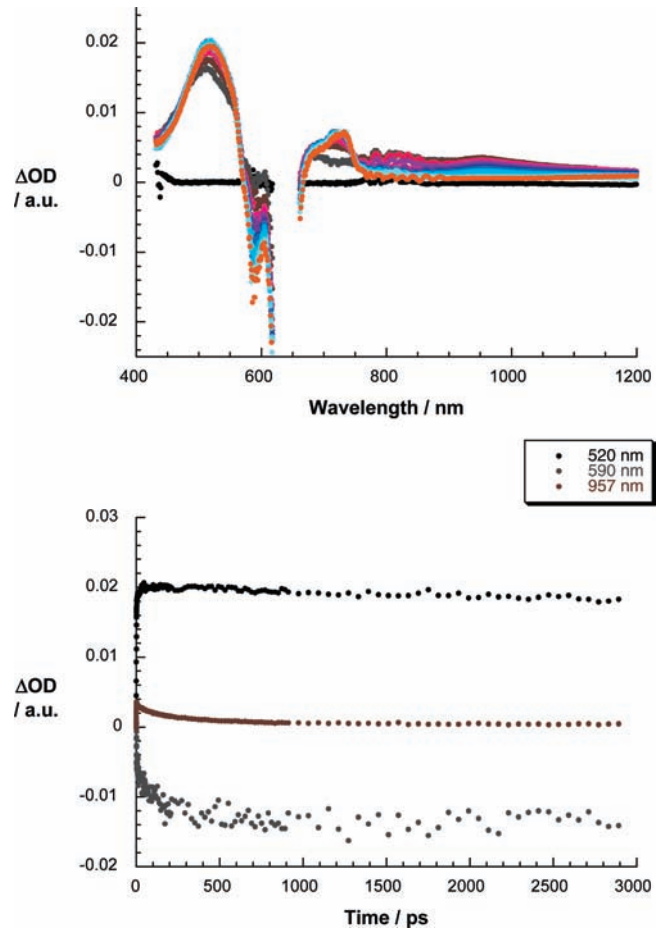

Figure 8. Top: differential absorption spectra (visible and near-infrared) obtained upon femtosecond flash photolysis (387; 150 nJ) of **5** (10 μM) in toluene with several time delays between 0 and 500 ps at room temperature. Bottom: time−absorption profile of the spectra shown above at 520 nm (black spectrum), 590 nm (gray spectrum), and 957 nm (brown spectrum), reflecting the charge separation and charge recombination.

in **4** the growth dynamics are much slower—1.0×10^{10} s^{-1}. A likely scenario involves a singlet−singlet energy transfer to afford the C_{60} singlet excited state, which, in turn, is the inception of the charge transfer. Support for this notion comes from a kinetic consideration, that is, comparing the charge transfer rate constants upon 387 and 660 nm excitation: They are virtually identical. Nevertheless, besides the $C_{60}^{\bullet-}$/$RuPc^{\bullet+}$ radical ion pair states, the RuPc triplet excited states are also formed. This finding is rationalized on the basis that the radical ion pair state energy (1.36 eV) is nearly isoenergetic with the RuPc triplet excited state (~1.3 eV). Notably, in **5** the presence of C_{60} does not exert any changes onto the RuPc decay dynamics. In this particular case, we postulate that the radical ion pair state (1.94 eV) is located above that of the RuPc singlet excited state (1.88 eV), which renders an intramolecular charge transfer endothermic.

All radical pair attributes are stable on the femto/picosecond time scale. The only exception is **5**, where lifetimes of 370 and 500 ps were determined in toluene and anisole, respectively; see Figure 8. The product of the rapid charge recombination is not the singlet ground state but the RuPc triplet excited state (~1.3 eV). Note that the solvent dependence suggests a moderately exothermic charge recombination (0.64 eV) that is placed in the normal region of the Marcus parabola. To examine the charge recombination dynamics, the same donor−acceptor hybrid solutions were excited with a 6 ns laser pulse at 355 nm. The transient absorption changes, recorded about 50 ns after the 6 ns laser excitation, reveal the attributes for the one-electron-oxidized RuPc and the one-electron-reduced fullerene; see Figures 9 and 10.

The decays of both probes resemble each other and give rise to kinetics that obey a clean unimolecular rate law. In toluene, the radical ion pair state lifetimes are 170 ns (**3**) and 130 ns (**4**) regardless of the presence or absence of molecular oxygen—a trend that confers a strongly exothermic charge recombination (1.35 and 1.16 eV) with kinetics in the inverted region of the Marcus parabola. Similarly, in anisole the lifetimes become shorter—150 ns (**3**) and 120 ns (**4**).

Conclusions

To summarize, we have demonstrated that coordination of pyridyl-based ligands to ruthenium(II) phthalocyanines is a powerful tool to assemble orthogonal donor−acceptor arrays in an efficient and versatile manner. The phthalocyanine and fullerene electroactive components of such complexes show electronic coupling in the ground state, as evidenced by UV/vis spectroscopy and electrochemical studies. The electronic distribution in hybrids **3** and **5** is strongly influenced by the presence of the powerful π-acceptor carbonyl ligand on one of the axial positions of the ruthenium phthalocyanine, so that the

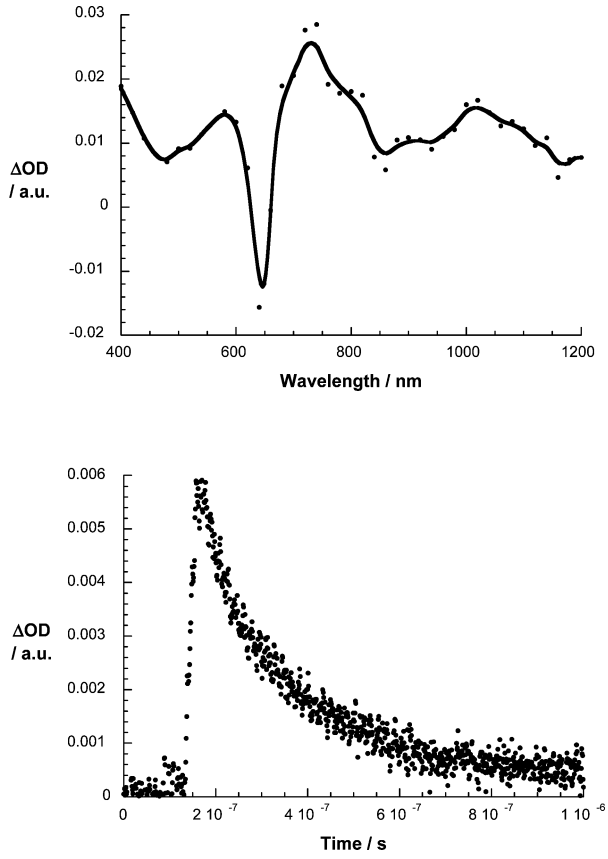

Figure 9. Top: differential absorption spectrum (visible and near-infrared) obtained upon nanosecond flash photolysis (355 nm) of **3** in oxygen-saturated toluene (10 μM) with a time delay of 50 ns at room temperature. Bottom: time−absorption profile of the spectrum shown above at 1020 nm, reflecting the charge recombination.

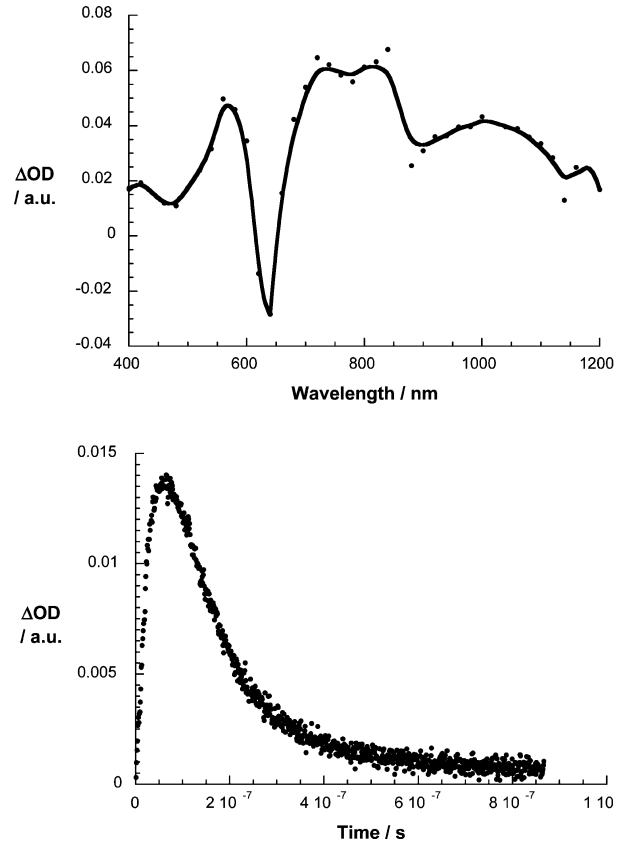

Figure 10. Top: differential absorption spectrum (visible and near-infrared) obtained upon nanosecond flash photolysis (355 nm) of **4** in oxygen-saturated toluene (10 μM) with a time delay of 50 ns at room temperature. Bottom: time−absorption profile of the spectrum shown above at 1020 nm, reflecting the charge recombination.

Pc ligand in complexes **3**, **5**, and **8** shows less reducing ability. Conversely, the fulleropyrrolidine moiety has shown efficient electron donor character, evident from the redox behavior of the triad **4**, where the Pc moiety is more and less prone to get oxidized and reduced, respectively. In the excited state, the behavior of these systems is dominated by the mono- or hexakis-substitution of the C_{60} component, rather than by the ratio of the donor or acceptor electroactive units. Thus, RuPc/C_{60} electron donor−acceptor hybrids have emerged as a versatile platform to fine-tune the outcome and dynamics of charge-transfer processes. A real asset is, in this context, the use of RuPc—rather than ZnPc—with a high-lying triplet excited state. In other words, the energy wasting and unwanted charge recombination have been successfully suppressed—with radical ion pair state lifetimes on the order of hundreds of nanoseconds for the monosubstituted C_{60} adducts **3** and **4**—by pushing them far into the inverted region. A comparison between the dyad **3** and the triad **4** containing the same motif reveals charge-separated-state lifetimes in the same range with kinetics that obey a clean unimolecular rate law. Furthermore, a powerful strategy arises from the unique hexakis-C_{60} functionalization, which shifts the reduction potential cathodically and, in turn, raises the radical ion pair state energy. Nevertheless, the location of the localized triplet excited state (i.e., RuPc) is not high enough. In fact, it still offers a rapid deactivation of the radical ion pair state. Thermodynamic considerations suggest dynamics that are nearly activationless—a hypothesis that is well corroborated by experimental results.

Experimental Section

General Procedures. 1. Synthesis. UV/vis spectra were recorded with a Hewlett-Packard 8453 instrument. IR spectra were recorded with a Bruker Vector 22 spectrophotometer. FAB-MS spectra were determined on a VG AutoSpec instrument. MALDI-TOF and ESI Q-TOF MS spectra were recorded with Bruker Reflex III and QSTAR spectrometers, respectively. NMR spectra were recorded with Bruker AC-300 and Bruker DRX-500 instruments. Column chromatography was conducted on silica gel Merck-60 (230−400 mesh, 60 Å) and Biobeads SX-3. TLC was performed on aluminum sheets precoated with silica gel 60 F_{254} (E. Merck). $Ru_3(CO)_{12}$ was purchased from Strem. Tetra-*tert*-butylphthalocyanine and all the other chemicals were purchased from Aldrich Chemical Co. and used as received without further purification.

2. Photophysics. Femtosecond transient absorption studies were performed with 387 and 660 nm laser pulses (1 kHz, 150 fs pulse width) from an amplified Ti:sapphire laser system (model CPA 2101, Clark-MXR Inc.). Nanosecond laser flash photolysis experiments were performed with 355 nm laser pulses from a Quanta-Ray CDR Nd:YAG system (6 ns pulse width) in a front face excitation geometry. Steady-state fluorescence measurements were performed by using a Fluoromax 3 (Horiba Jobin Yvon). The experiments were performed at room temperature.

3. Electrochemistry. Voltammetric experiments were performed on a potentiostat/galvanostat, model CHI660A (CH Instruments electrochemical workstation), with a three-electrode cell placed in a Faraday cage. A GC disk with a diameter of 1.00 mm

(Bioanalytical Systems Inc.) was used as the working electrode. The surface of the electrode was polished using extrafine carborundum paper (Buehler) followed by 0.3 μm alumina and 0.25 μm diamond polishing compound (Metadi II, Buehler). The electrode was then sonicated in water to remove traces of alumina from the metal surface, washed with water, and dried. The counter electrode was made from platinum mesh (0.25 mm) and was cleaned by heating in a flame for approximately 30 s. A silver wire immersed in 0.01 mol L^{-1} silver nitrate and 0.09 mol L^{-1} $(n\text{-Bu})_4PF_6$ in acetonitrile and separated from the analysis solution by a ceramic tip (Bioanalytical System Inc.) served as the reference electrode. The silver hexafluorophosphate solution was replaced daily, because of the instability of Ag^+ to photoreduction. The stability of the reference electrode was examined by recording the ferrocene oxidation potential in the solvent studied as a function of time. The formal potential of the ferrocene−ferrocenium system was found to be stable for about 12 h. The solution was deaerated for 20 min with argon prior to the electrochemical measurements.

Synthesis of Pyridylpyrrolidino-C_{60}-Tetramalonate Monoadducts 13 and 14. A round-bottom flask was charged with C_{60}-tetramalonate (0.200 g, 0.15 mmol), *N*-(4-pyridyl)glycine (0.337 g, 2.02 mmol), and paraformaldehyde (0.218 g, 7.25 mmol). To this was added 1,2-dichlorobenzene (120 mL), and the resulting mixture was refluxed under Ar for 3 h. The resulting mixture was cooled and the solvent evaporated. The resulting residue was loaded onto a silica column using 1% MeOH in CH_2Cl_2 as the eluent. The column was allowed to drip via gravity (no flashing). A green/brown band was isolated (unreacted C_{60}-tetramalonate). The polarity was then increased to 2% MeOH to remove an orange impurity band. The polarity was finally increased to 3% MeOH, which eluted a long, streaky band with an orange front and a yellow tail. Test tube fractions of this band were collected. The orange bands were combined to give unsymmetrical monoadduct, while the yellow bands were combined to give symmetric monoadduct **13** (15 mg, 25% yield based on consumed C_{60}-tetramalonate). The two isomers were formed in roughly a 1:1 ratio (by ^{1}H NMR integration). Data for **13**: ^{1}H NMR (300 MHz, $CDCl_3$) δ = 8.34 (br d, 2H, $H^{2',6'}$), 6.72 (br d, 2H, $H^{3',5'}$), 4.32−4.43 (m, 20H, H^{Pyrr}, OCH_2CH_3), 1.30−1.40 (m, 24H, OCH_2CH_3). Data for **14**: ^{1}H NMR ($CDCl_3$) δ = 8.39 (br d, 2H, $H^{2',6'}$), 6.72 (br d, 2H, $H^{3',5'}$), 4.31−4.78 (m, 20H, H^{Pyrr}, OCH_2CH_3), 1.33−1.51 (m, 24H, OCH_2CH_3).

Synthesis of *trans*-1-Bis[*N*-(4-pyridyl)fulleropyrrolidine] Tetramalonate Ligand 2. To a round-bottom flask were added **13** (0.063 g, 0.04 mmol), *N*-(4-pyridyl)glycine (0.130 g, 0.86 mmol), and paraformaldehyde (0.026 g, 0.86 mmol). To this was added 1,2-dichlorobenzene (40 mL), and the resulting mixture was refluxed under Ar for 4 h. The reaction was monitored every 4 h by TLC (5% MeOH in CH_2Cl_2). More pyridylglycine and paraformaldehyde were added in the amounts above, and the reflux was continued for 4 h. This was repeated until all monoadduct was consumed and bisadduct had grown in (as seen in TLC). When the reaction was complete, the mixture was cooled and the solvent evaporated. The residue was loaded onto a column with 3% MeOH in CH_2Cl_2 as the eluent to remove any remaining monoadduct. The polarity was increased to 5% MeOH, and the band containing bisadducts was isolated. This material was purified via preparative TLC by running the plate with 4% MeOH in CH_2Cl_2, drying, running the plate again with 5% MeOH, drying, and finally running with 6% MeOH. The resulting band had a yellow head and orange tail. The yellow head was carefully removed, and the remainder of the band was taken off the silica and subjected to the same chromatography until no more yellow was eluting on the plate. The combined yellow fractions on silica were sonicated in 5% MeOH in CH_2Cl_2, the liquid was decanted off through a fritted funnel, and the process was repeated until all of the material was removed from the silica. The filtrate was evaporated, and hexane was added. The resulting mixture was filtered through a syringe fitted with a Teflon filter. CH_2Cl_2 was then added to dissolve residue, and this was run through the syringe/filter. The solvent was evaporated to give pure **2** (0.006 g) as a yellow solid (9% yield from **13**): ^{1}H NMR (300 MHz, $CDCl_3$) δ = 8.40 (d, 4H, $H^{2',6'}$), 6.84 (d, 4H, $H^{3',5'}$), 4.66 (s, 8H, H^{Pyrr}), 4.28−4.33 (2q, 16H, OCH_2CH_3), 1.25−1.33 (2t, 24H, OCH_2CH_3); UV/vis ($CHCl_3$) λ_{max} (log ε) = 285 (4.77) nm; MS (MALDI-TOF, dithranol) m/z = 1592 $[M]^+$.

Bisacetonitrile[2(3),9(10),16(17),23(24)-tetrakis-*tert*-butylphthalocyaninato]ruthenium(II) (7). The irradiation was carried out in an immersion well apparatus with a Pyrex filter and a 120 W medium-pressure Hg arc lamp. A solution of the phthalocyanine precursor **6** (50 mg, 0.058 mmol) in acetonitrile (200 mL) was purged for 1 h with argon and irradiated under a positive pressure of argon for 1 h. The reaction course was monitored by TLC. After completion, the solvent was evaporated under reduced pressure and the residue was chromatographed on silica gel using dichloromethane as the eluent. The blue solid was suspended in pentane, filtered, and washed with the same solvent to afford 50 mg (94%) of **7** as a blue solid: ^{1}H NMR (300 MHz, $CDCl_3$) δ = 9.30 (d, 4H, H arom), 9.2−9.1 (m, 4H, H arom), 8.00 (d, 4H, H arom), 1.78, 1.77, 1.76, 1.75 (4 s, 36H, $C(CH_3)_3$), −0.17 (s, 6H, CH_3CN); ^{13}C NMR (75.5 MHz, $CDCl_3$) δ = 151.32, 151.30, 151.29, 144.20, 144.18, 144.12, 144.09, 140.70, 140.68, 140.64, 140.62, 138.29, 125.24, 125.19, 120.89, 120.86, 120.82, 120.77, 120.73, 117.76, 117.74, 117.73, 117.69, 117.65, 117.63, 117.61, 108.9, 108.32, 108.28, 35.62, 35.59 (2 $C(CH_3)_3$), 32.10, 32.07 (2 $C(CH_3)_3$), 1.20 (CH_3CN); IR (KBr) ν = 3061 (CH arom), 2953, 2910, 2872 (C−H), 1718, 1651, 1610, 1462, 1394, 1367, 1259, 1192, 1151, 1111, 1043, 941, 835, 760, 692 cm^{-1}; UV/vis ($CHCl_3$) λ_{max} (log ε) = 317 (4.77), 592 (4.19), 652 (4.48) nm; MS (ESI-TOF, MeOH + 1% TFA) m/z = 915−923 $[M]^+$.

Carbonylpyridyl[2(3),9(10),16(17),23(24)-tetrakis-*tert*-butylphthalocyaninato]ruthenium(II) (8). A solution of **6** (50 mg, 0.058 mmol) in pyridine (3 mL) was stirred at room temperature for 5 min. The solvent was evaporated under reduced pressure, and the residue was chromatographed on silica gel using toluene as the eluent to give **8** (46 mg, 54%) as a blue solid: ^{1}H NMR (300 MHz, $CDCl_3$) δ = 9.45 (d, 4H, H arom), 9.3−9.2 (m, 4H, H arom), 8.15 (dd, 2H, H arom), 8.13 (dd, 2H, H arom), 6.1−6.0 (m, 1H, $H^{4'}$), 5.3−5.2 (m, 2H, $H^{3'}$, $H^{5'}$), 2.04 (d, J = 5 Hz, 2H, $H^{2'}$, $H^{6'}$), 1.79, 1.78, 1.77 (3 s, 36H, $C(CH_3)_3$); ^{13}C NMR (125.8 MHz, $CDCl_3$) δ = 179.24 (CO), 152.58, 152.54, 150.01, 144.29, 144.27, 139.83, 139.75, 137.41, 137.38, 135.26, 129.03, 128.22, 126.47, 126.44, 126.42, 126.38, 122.84, 122.33, 121.74, 121.71, 121.69, 118.57, 118.53, 35.83, 35.80 (2 $C(CH_3)_3$), 32.05, 32.01 (2$C(CH_3)_3$); IR (KBr) ν = 3069 (CH arom), 2962, 2922, 2868 (C−H), 1969 (CO), 1618, 1483, 1389, 1362, 1323, 1283, 1256, 1157, 1117, 1090, 1049, 935, 827, 764, 690 cm^{-1}; UV/vis ($CHCl_3$) λ_{max} (log ε) = 296 (5.01), 345 (4.53), 590 (4.42), 627 (sh), 652 (5.18) nm; MS (MALDI-TOF, dithranol) m/z = 863−869 $[M - Py + H]^+$, 835−841 $[M - CO - Py + H]^+$.

[Ru(CO)(C_{60}Py)Pc] (3). A solution of phthalocyanine **6** (10 mg, 0.011 mmol) and fullerene ligand **1** (10 mg, 0.011 mmol) in toluene (2 mL) was stirred at room temperature and protected from light for 24 h. After this time, the reaction was complete, as monitored by TLC. The solvent was evaporated, and the crude was chromatographed on Biobeads SX-3 using toluene as the eluent. The second fraction was suspended in methanol, filtered, and washed first with the same solvent and then with hexanes. The obtained solid was dried at 10^{-1} mmHg to yield **3** (15 mg, 80%) as a blue solid: ^{1}H NMR (300 MHz, $CDCl_3$) δ = 9.46 (dd, 2H, H arom), 9.43 (dd, 2H, H arom), 9.3−9.2 (m, 4H, H arom), 8.17 (dd, 2H, H arom), 8.14 (dd, 2H, H arom), 4.95 (d, J = 7 Hz, 2H, $H^{3'}$, $H^{5'}$), 4.20 (s, 4H, H^{Pyrr}), 1.87 (d, 2H, J = 7 Hz, $H^{2'}$, $H^{6'}$), 1.80, 1.79, 1.78 (4 s, 36H, $C(CH_3)_3$); ^{13}C NMR (125.8 MHz, $CDCl_3$) δ = 178.81 (CO), 152.45, 152.39, 149.90, 147.27 146.13, 145.97, 145.32, 145.24, 145.16, 144.88, 144.27, 144.25, 144.11, 144.04, 142.87, 142.50, 141.84, 141.71, 141.64, 139.91, 139.82, 137.52, 137.47, 135.44, 126.35, 121.71, 118.52, 107.83, 68.34, 58.67, 36.05, 35.83, 35.79 (3 $C(CH_3)_3$), 32.07, 32.05 (2 $C(CH_3)_3$); IR (KBr) ν = 3069 (CH arom), 2949, 2922, 2854 (C−H), 1969 (CO), 1607, 1481, 1387,

1360, 1321, 1258, 1219, 1148, 1121, 1094, 1053, 1014, 933, 827, 766, 692, 669 cm^{-1}; UV/vis (toluene) λ_{max} (log ε) = 302 (5.17), 351 (4.67), 435 (3.35) 588 (4.50), 628 (sh), 650 (5.22) nm; MS (MALDI-TOF, dithranol) m/z = 1674−1682 $[M - CO]^+$, 1668−1684 $[(PcRu)_2]^+$, 860−870 $[(CO)PcRu]^+$, 841 $[C_{60}Py + H]^+$, 832−842 $[PcRu]^+$.

[Ru(C_{60}Py)$_2$Pc] (4). A solution of **7** (8 mg, 0.008 mmol) and **1** (14 mg, 0.016 mmol) in toluene (4 mL) was heated at 60−80 °C for 1 h. After this time, the reaction was complete, as monitored by TLC. The solvent was rotary evaporated, and the residue was chromatographed on Biobeads SX-3 using toluene as the eluent. After evaporation of the second fraction, the solid was suspended in methanol, filtered, and washed with the same solvent and then with pentane to afford **4** (12 mg, 58%) as a blue solid: ^{1}H NMR (300 MHz, $CDCl_3$) δ = 9.23 (d, 4H, H arom), 9.1−9.0 (m, 4H, H arom), 7.96 (d, 4H, H arom), 5.00 (d, J = 6 Hz, 4H, H$^{3'}$, H$^{5'}$), 4.23 (s, 8H, H^{Pyrr}), 2.51 (d, 4H, J = 6 Hz, H$^{2'}$, H$^{6'}$), 1.76, 1.75 (2 s, 36H, C(CH_3)$_3$); ^{13}C NMR (125.8 MHz, $CDCl_3$) δ = 152.74, 149.78, 149.74, 149.73, 147.33, 146.20, 145.39, 145.22, 145.10, 144.35, 142.93, 142.56, 141.94, 141.86, 141.73, 139.98, 135.60, 133.12, 125.26, 108.17, 68.63, 58.96, 35.60, 35.56 (2 *C*(CH_3)$_3$), 32.12, 32.09 (2 C(*C*H$_3$)$_3$); IR (KBr) ν = 3069 (CH arom), 2957, 2866 (C−H), 1720, 1609, 1464, 1396, 1356, 1315, 1248, 1221, 1153, 1113, 1086, 1045, 1018, 829, 760 cm^{-1}; UV/vis (toluene) λ_{max} (log ε) = 321 (5.25), 381 (sh), 437 (4.16) 576 (4.39), 631 (4.79) nm; MS (MALDI-TOF, dithranol) m/z = 2513−2525 $[M]^+$, 1668−1684 $[(PcRu)_2]^+$, 841 $[C_{60}Py + H]^+$, 832−842 $[PcRu]^+$.

[Ru$_2$(CO)$_2$(C_{60}Py$_2$)Pc$_2$] (5). A solution of **6** (7 mg, 0.008 mmol) and **2** (6 mg (0.004 mmol) in chloroform (2 mL) was stirred at room temperature and protected from light for 20 h. The solvent was rotary evaporated, and the residue was chromatographed on Biobeads SX-3 using toluene as the eluent. The first fraction was evaporated, suspended in methanol, filtered, and washed with the same solvent and then with pentane to afford **5** (9 mg, 65%) as a blue solid: ^{1}H NMR (300 MHz, $CDCl_3$) δ = 9.39 (dd, 4H, H arom), 9.37 (dd, 4H, H arom), 9.3−9.2, (m, 8H, H arom), 8.11 (dd, 4H, H arom), 8.08 (dd, 4H, H arom), 4.58 (d, J = 7 Hz, 4H, H$^{3'}$, H$^{5'}$), 4.1−4.0 (m, 16H, OC*H*$_2$CH$_3$), 3.51 (s, 8H, H^{Pyrr}), 1.77, 1.76, 1.75, 1.74 (4 s, 72H, C(CH_3)$_3$), 1.69 (d, 4H, J = 7 Hz, H$^{2'}$, H$^{6'}$), 1.1−1.0 (m, 24H, OCH$_2$C*H*$_3$); ^{13}C NMR (125.8 MHz, $CDCl_3$) δ = 178.77 (CO), 163.46, 163.07, 162.94, 162.43 (COO), 151.17, 149.63, 149.27, 145.65, 145.63, 145.61, 144.56, 144.28, 144.24, 144.22, 144.20, 144.19, 144.12, 144.09, 144.05, 144.04, 144.02, 143.96, 142.87, 139.90, 139.82, 139.31, 137.87, 137.51, 137.46, 129.03, 128.22, 126.25, 126.21, 126.17, 125.29, 121.66, 121.63, 118.51, 118.47, 118.46, 118.45, 118.43, 107.42, 70.37, 66.42, 64.92, 62.61, 62.59, 62.57, 57.29, 44.47, 35.78, 35.74 (2 *C*(CH_3)$_3$), 32.05, 32.01 (2 C(*C*H$_3$)$_3$), 13.93, 13.90, 13.86, 13.85 (4 OCH$_2$*C*H$_3$); IR (KBr) ν = 2955, 2862 (C−H), 1971 (CO), 1740 (COO), 1612, 1485, 1462, 1393, 1369, 1323, 1254, 1219, 1149, 1119, 1092, 1045, 1022, 802, 756 cm^{-1}; UV/vis ($CHCl_3$) λ_{max} (log ε) = 305 (5.40), 351 (sh), 591 (4.78), 628 (sh), 650 (5.48) nm; MS (MALDI-TOF, dithranol) m/z = 1668−1684 $[(PcRu)_2]^+$,1593 $[C_{60}Py_2 + H]^+$, 860−870 $[(CO)PcRu]^+$, 832−842 $[PcRu]^+$.

Acknowledgment. Funding from MEC and MICINN (CTQ2008-00418/BQU, CONSOLIDER-INGENIO 2010 CDS2007-00010 Nanociencia Molecular, FOTOMOL, PSE-120000-2008-3), ESF-MEC (MAT2006-28180-E, SOHYDS), EU (Solar-N-type, MRTN-CT-2006-035533, ROBUST DSC, FP7-Energy-2007-1-RTD, N° 212792), COST Action D35, and CAM (MADRISOLAR, S-0505/PPQ/000225), the Deutsche Forschungsgemeinschaft (Grant SFB 583), FCI, and the Office of Basic Energy Sciences of the U.S. Department of Energy is gratefully acknowledged. M.S.R.-M. and E.C. also acknowledge MEC (Spain) for a Ramón y Cajal research position and a postdoctoral contract, respectively. This material is based on work supported by the National Science Foundation (Grant DMR-0809129 to L.E.) while L.E. was working at the Foundation.

Supporting Information Available: Complete refs 2c and 14d and characterization data for compounds **2**−**5**, **7**, and **8** (^{1}H NMR, ^{13}C NMR, UV/vis, MS, and electrochemical redox potentials from CV experiments). This material is available free of charge via the Internet at http://pubs.acs.org.

JA902471W